Patterns of Flow in the Canyons of the Northern Gulf of Alaska

Calvin W. Mordy[a, b*], Phyllis J. Stabeno[b], Nancy B. Kachel[a, b], David Kachel[b]
Carol Ladd[b], Mark Zimmermann[c], Albert Hermann[a, b], Kenneth Coyle[d], and
Miriam J. Doyle[a, c]

[a]Joint Institute for the Study of the Atmosphere and Ocean, University of Washington, 3737 Brooklyn Ave NE, Box 355672, Seattle, WA 98105-5672 USA
Mordy@u.washington.edu, Phone: (206) 526-6870
Nancy.Kachel@noaa.gov, Phone: (206) 526-6746
Miriam.Doyle@noaa.gov, (206) 526-4318

[b]Pacific Marine Environmental Laboratory, NOAA, 7600 Sand Point Way, NE, Seattle WA 98115 USA
Phyllis.Stabeno@noaa.gov, Phone: (206) 526-6453
Carol.Ladd@noaa.gov, Phone: (206) 526-6024

[c]National Marine Fisheries Service, NOAA, 7600 Sand Point Way, NE, Seattle WA 98115 USA
Mark.Zimmermann@noaa.gov, Phone: (206) 526-4119

[d]Institute of Marine Science, University of Alaska, Fairbanks, AK 99775-7220, USA

*Corresponding Author

For: Deep Sea Research II

ABSTRACT

The continental shelf around Kodiak Island is incised with numerous submarine canyons, which play an important role in the cross-shelf transport of heat, salt, and nutrients, and the transport of ichthyoplankton of deep-spawning fish from the slope region into the shallow nursery grounds surrounding Kodiak Island. To explore the pathways and variability of flow, and the extent of tidal mixing within the canyons, moorings were placed in the Chiniak, Barnabas, and Amatuli troughs, and off the shelf from Resurrection Bay (Seward Line) and the Kenai Peninsula (Gore Point). In the troughs, intensified flow was evident near the trough walls, and flow was directed by bathymetry with inflow along the upstream (northern) side and outflow along the downstream (southern) side. The presence of mesoscale eddies in the gulf had no unique influence on currents or salinity in the troughs. Tidal mixing was strongest in Chiniak Trough, and this introduced cold, nutrient-rich bottom waters into the upper water column. Intensified bottom flow associated with the Alaskan Coastal Current was evident along the Seward Line and Gore Point, and directed toward the Kennedy-Stevenson Entrances, which are also regions of strong tidal mixing. Observations of tidal mixing were consistent with model results and satellite images showing cooler, phytoplankton-rich water in summer in the nursery grounds that surround Kodiak Island. Patterns of flow within the troughs and in Shelikof Strait were consistent with the springtime advance of ichthyoplankton across the shelf.

1. Introduction

Basin circulation in the Gulf of Alaska (GOA) is dominated by the Subarctic Gyre (Favorite and Ingraham, 1977; Reed, 1984; Reed and Stabeno, 1989). The gyre is bounded to the south by the West Wind Drift, which bifurcates into the California and Alaska Currents at the west coast of North America. The northward flowing Alaska Current is a broad eastern boundary current that often contains large mesoscale eddies. At the northern part of the basin, the Alaska Current turns to the southwest and intensifies into the Alaskan Stream, a western boundary current that flows along the slope and continues southwestward along the Aleutian Arc.

Flow over the shelf is dominated by the Alaska Coastal Current (ACC), a coastal current forced by downwelling winds with a strong freshwater component (Stabeno et al., 2004, 2016a, 2016b). Freshwater in the ACC is derived from a line source of rivers and rivulets that drain the large watersheds of the coastal and inland mountains. The maximum freshwater input occurs in late summer due to the melting snowpack and increasing rainfall associated with the autumn transition (Royer, 1982; Weingartner et al., 2005). This results in a freshwater cap on the inner shelf that can restrict diapycnal mixing and vertical diffusion of deeper, more nutrient-rich water into the photic zone during late summer and early autumn (Stabeno et al., 2004, 2016a).

The ACC flows northward along the eastern GOA, is disrupted and directed seaward at Kayak Island, and redevelops farther west with a freshwater core that includes water exiting Prince William Sound (Stabeno et al., 2016a, 2016b). The ACC flows along the south side of Kenai Pennisula and bifurcates in the vicinity of the Barren Islands (which lie between Kennedy and Stevenson Entrance). In autumn and winter, the flow of the ACC is strong (1.4×10^6 m^3 s^{-1}), with ~70% of the volume directed down Shelikof Strait (Stabeno et al., 2016a). In summer, the

42 flow is weaker (0.6×10^6 m^3 s^{-1}), and ~60% of the volume remains on the seaward side of
43 Kodiak Island.

44 The northern Gulf of Alaska (NGOA) is predominately a downwelling-favorable system,
45 with downwelling-favorable winds dominating from September through April and neutral
46 (neither up- nor downwelling) wind conditions persisting over the rest of the year (Stabeno et al.,
47 2004; Strom et al., 2006). On weekly time scales, however, periods of upwelling can occur
48 during spring and summer (Hermann et al., 2009, Stabeno et al., 2004; Strom et al., 2006).
49 Despite these conditions, the shelf is considered to be a highly productive ecosystem with annual
50 production of ~300 g C m^{-2} yr^{-1} (Sambrotto and Lorenzen, 1986), which supports large
51 populations of fish, mammals, and invertebrates (Calkins, 1986; Mundy, 2005; OCSEAP, 1986).

52 In the basin, primary production is limited by iron availability while over the shelf, iron is
53 generally replete and primary production is nitrate limited (Boyd et al., 2004; Aguilar-Islas et al.,
54 2016). Iron limitation on the shelf has been reported due to high ligand concentrations (Strom et
55 al., 2016), and ROMS models suggest that much of the outer shelf off the Kenai Peninsula and
56 the south coast of Kodiak Island is iron limited, especially in spring (Coyle et al., 2012).
57 Mesoscale eddies, which often occur along the slope and in the basin, can promote shelf-basin
58 exchange including the exchange of limiting nutrients into each domain thereby enhancing
59 primary production (Aguilar-Islas et al., 2016; Ladd et al., 2007). Satellite imagery indicates
60 higher levels of chlorophyll associated with mesoscale eddies in the central GOA (Brickley and
61 Thomas, 2004; Ladd et al., 2005b, 2007).

62 The spring phytoplankton bloom is regulated primarily by light availability, and typically
63 occurs in April–May when the shelf begins to thermally stratify (Henson, 2007; Strom et al.,
64 2006; 2016). The spring bloom commonly encompasses the shelf and portions of the basin

65 (Stabeno et al., 2004; Brickley and Thomas, 2004). Post-bloom production is limited for much of
66 the ecosystem, as mid- and inner shelf waters are generally nitrogen limited throughout the
67 summer (Stabeno et al, 2004; Strom et al., 2006). However, satellite chlorophyll imagery
68 suggests that post-bloom production is sustained in waters around the Kodiak Archipelago
69 (Brickley and Thomas, 2004; Stabeno et al., 2004). In lieu of traditional nutrient upwelling via
70 Ekman transport, other mechanisms of nutrient pumping must be operative off Kodiak Island to
71 sustain summer production (Stabeno et al., 2004; Ladd et al., 2005a; Hermann et al., 2009).
72 Compared to the narrow shelf of the eastern gulf (east of ~145°W), the shelf in the
73 northern and western gulf is relatively wide and incised with multiple canyons and troughs,
74 which are separated by shallow banks. Right-bounded flows, such as occur in the GOA basin,
75 interact with canyons in several ways (Spurgin and Allen, 2014). One pattern has a trapped anti-
76 cyclonic flow within the canyon resulting in little onshore flow (Flexas et al., 2008). A second
77 pattern which we observe in the GOA has slope flow entering the canyon and following
78 bathymetry along the canyon walls (Klinck, 1996).
79 Stabeno et al. (2004, 2016a) hypothesized that it was the interplay of canyons and tidal
80 mixing that resulted in the high productivity of the Kodiak Archipelago in summer. They
81 suggested that nutrient-rich slope water was transported up the canyons and introduced to the
82 upper water column by strong tidal mixing at the head and along the sides of the canyons,
83 thereby sustaining post-bloom production. To test this hypothesis, Ladd et al. (2005a) used
84 mooring data to demonstrate the occurrence of onshore flow through valleys and canyons on
85 tidal to weekly scales, and in addition provided evidence of deep tidal mixing that introduced this
86 water into the photic zone. This process was clearly demonstrated in high-resolution (3 km)
87 coupled ROMS-NPZ (Regional Ocean Modeling System–Nutrients, Phytoplankton and

88 Zooplankton) models in the NGOA (Cheng et al., 2012; Hermann et al., 2009). Not only do the
89 canyons foster cross-shelf exchange of slope water (e.g., nutrients and salt), but they also serve
90 as important conduits in the transport of several important larval species from their spawning
91 grounds near the slope to nursery areas in shallow bays and estuaries near Kodiak Island (Bailey
92 et al., 2008; Doyle and Mier, 2016).

93 Previous efforts have identified regions and mechanisms of cross-shelf flow, larval
94 transport, and vertical nutrient flux, but there has not been a comparison of physical processes in
95 the different canyons surrounding Kodiak Island. We use data from moorings and hydrographic
96 surveys along with results from a coupled biophysical model to compare mixing in several
97 canyons, and elucidate patterns and variability of bottom flow around Kodiak Island. Three
98 major bathymetric features in the western GOA are investigated; Amatuli Trough, Chiniak
99 Trough, and Barnabas Trough (Fig. 1). High-resolution bathymetry maps are provided for each
100 bathymetric feature along with net bottom flow at the mooring locations. While a subset of
101 moored current data has previously been published (Stabeno et al., 2004; Ladd et al., 2005a),
102 data from 29 moorings are used to determine patterns of bottom flow in the NGOA. An 18-year
103 record of currents in Chiniak Bay is used to examine daily, seasonal and interannual variability
104 of bottom flow into the Bay. Moored temperature strings facilitate a comparison of mixing in
105 Chiniak and Barnabas Troughs, and time series of currents and salinity are used to examine the
106 influence of mesoscale eddies on flow in Amatuli Trough. Some of these observations are
107 compared with results obtained from a nested biophysical model. The ingress of larvae on to the
108 shelf is observed in association with canyons which connect deep water-spawning locations with
109 coastal juvenile nursery grounds.

110 **2. Methods**

111 *2.1 Bathymetry*

112 Bathymetry data were downloaded from the National Geophysical Data Center (NGDC:
113 http://www.ngdc.noaa.gov), proofed against the source maps, edited, digitized, and shifted to a
114 modern datum (NAD83 : North American Datum of 1983). Geographic Information System
115 (GIS) methods are described in Zimmermann and Benson (2013), and the specific data sets
116 utilized for this central GOA compilation are described in Zimmermann and Prescott (2015).
117 Edited bathymetry data (the individual points, or soundings) were converted into a continuous
118 network of triangles (TIN: Triangular Irregular Network) with the soundings as corners of the
119 triangles. Then the TIN was converted by linear interpolation into a raster surface of 100 m sized
120 cells.

121 *2.2 Moored Currents, Temperature, and Salinity*

122 Subsurface moorings were all taut-wire, measuring temperature (Sea-Bird SBE-37 and
123 SBE39, Aanderaa RCM-9 current meters), salinity (SBE-37 and SBE-41), and currents (RCM-7,
124 RCM-9, and Teledyne RDI acoustic Doppler current profilers—ADCP) at selected depths. Most
125 of the ADCP moorings consisted of an upward looking 300 kHz instrument. All moored
126 oceanographic equipment was prepared and the data processed according to manufacturers'
127 specifications. Sampling on all instruments was at half-hourly or hourly intervals. Temperature
128 and salinity from the moored instruments were compared to nearby hydrographic casts for
129 calibration. Temperature was sampled hourly. Except for data in Table 1, current and salinity
130 time series were low-pass filtered with a 35 hr, cosine-squared, tapered Lanczos filter to remove
131 tidal and higher-frequency variability, and subsequently re-sampled at 6-hour intervals. In Table
132 1, unfiltered data was used, and eddy kinetic energy (KE') and kinetic energy of the mean flow
133 ($\overline{KE}$) per unit mass were calculated as:

$$KE' = \frac{(\sigma^2{}_u + \sigma^2{}_v)}{2} \quad (1)$$

$$\overline{KE} = \frac{(\bar{u}^2 + \bar{v}^2)}{2} \quad (2)$$

where $\sigma^2{}_u$ and $\sigma^2{}_v$ are the variance of u (eastward flow) and v (northward flow), respectively, and the mean flow is designated by $\bar{u}$ and $\bar{v}$. The ratio of $KE'/(\overline{KE} + KE')$ provides a measure of the variance of the flow (Stabeno et al., 1995), and when using unfiltered data, this ratio provides an indication of the fraction of energy due to tides. Note that current meter data used in Stabeno et al. (1995) were low-pass filtered to remove tidal signals.

2.3 Hydrographic Surveys

Conductivity/temperature/depth (CTD) data were obtained using a Sea-Bird 911-Plus CTD with dual temperature and conductivity sensors. Sensors were calibrated by the manufacturer. Salinities were verified from samples collected near the bottom on approximately every second cast, and analyzed on a salinometer that was calibrated with ISO standard water.

2.4 Satellite Sea Surface Height, Sea Surface Temperature, and Chlorophyll

Gridded sea surface height anomaly (SSHA) data were downloaded from AVISO (Archiving, Validation and Interpretation of Satellite Oceanographic data). The ‘‘all sat merged’’ dataset (obtained from http://www.aviso.altimetry.fr) consists of delayed-mode, merged data from up to four satellites at a given time. Anomalies are calculated with respect to a 20-year mean. AVISO applies an optimal interpolation methodology to merge data from multiple altimeters (Dibarboure et al., 2010; Le Traon et al., 1998). By using the maximum number of available satellites, sampling and long wavelength errors are improved, but the quality of the time series is not homogenous in time (Dibarboure et al., 2010). Merging data from multiple satellites with differing spatial and temporal resolution helps resolve mesoscale features,

allowing for a better description of eddy activity (Ducet et al., 2000; Le Traon and Dibarboure, 2004; Pascual et al., 2006). Assuming geostrophy, eddy kinetic energy (*EKE*, per unit mass) was estimated from the SSHA (η') as:

$$EKE = \frac{1}{2}\left[\left\langle U_g'^2 \right\rangle + \left\langle V_g'^2 \right\rangle\right] \quad (3)$$

$$U_g' = -\frac{g}{f}\frac{\Delta\eta'}{\Delta y}, V_g' = \frac{g}{f}\frac{\Delta\eta'}{\Delta x}, \quad (4)$$

where x is eastward and y is northward, $U'g$ and $V'g$ are the geostrophic velocity anomalies, f is the Coriolis parameter, and ‹ › denotes the time average [Ducet et al., 2000; Ladd, 2007].

Composite maps of sea-surface temperature (SST) and chlorophyll were created around Kodiak Island using data from the Modis Aqua satellite. Level 1A data files were obtained from NASA's Ocean Color website (http://oceancolor.gsfc.nasa.gov), and processed using SeaDAS (http://seadas.gsfc.nasa.gov/), a suite of programs created and maintained by NASA to process the files. Composites were constructed using the mean SST or chlorophyll at each pixel with a valid value from August 21 to 23 for SST and from August 1 to 13 for chlorophyll.

2.5 Winds

The North American Regional Reanalysis (NARR) was introduced as an extension to the National Centers for Environmental Prediction Reanalysis 2 (NCEPR2) for the North American Region using the high resolution NCEP Eta model (~32 km grid size compared to NCEPR2's 2.5° grid) and includes additional assimilated parameters to improve the reanalysis product (Mesinger et. al, 2006). Wind speeds (three-hourly) from May to December 2001 were downloaded at the location "NARR" indicated in Figure 1.

2.6 Coupled Biophysical Model

For comparisons with observations, as well as determination of typical Rossby Radius and Rossby Number values throughout the coastal GOA, we utilized a regional model of the GOA based on the Regional Ocean Modeling System (ROMS), with 3 km horizontal resolution and 42 vertical layers. The basic features of this model and its validation are described in Coyle et al. (2012, 2013); the version used here included recent upgrades to coastal runoff forcing (Coyle et al., submitted). Salient features for its use here include its explicit resolution of major tidal constituents, as well as vertical eddy diffusivities calculated from instantaneous vertical profiles of velocity and density.

Typical values of the first internal Rossby Radius scale (λ) at each horizontal gridpoint were calculated using the vertically averaged value of the buoyancy frequency ($\bar{N}$), the local depth (H) and potential density (ρ) and the local value of the Coriolis parameter (f):

$$N^2 = -(d\rho/dz)/\rho \quad (5)$$

$$\lambda = (\frac{\bar{N}H}{\pi})/f \quad (6)$$

Typical values of the Rossby Number (ε) at each horizontal gridpoint were calculated using the vertically averaged speed ($\bar{U}$), the length scale of the local bathymetry (L), and the local value of the Coriolis parameter (f) as:

$$\varepsilon = \bar{U} / f L \quad (7)$$

The length scale L at each location was calculated from the absolute value of the slope of the bathymetry normalized by the depth (i.e. the fractional change in depth with distance).

$$L = \langle \nabla H \rangle / H \quad (8)$$

Weekly averaged (and tidally filtered) density (ρ) and velocity ($\bar{U}$) fields were from mid-July of 2010.

199

200 **3. Results**

201 *3.1 Rossby Radius and Rossby Number*

202 Over the shelf, values of the first internal Rossby Radius scale ranged from near-zero to
203 10 km (Fig. 2). The lowest values were observed over the (tidally well-mixed) shallow banks,
204 and largest values were observed in the deepest canyons. This suggests that the primary length
205 scales of horizontal variability in the canyons (e.g. > 5 km) are resolved by the native grid. The
206 most energetic mesoscale features of the NGOA, such as the mesoscale eddies in Shelikof Strait,
207 have length scales of 30-40 km (Bograd et al., 1994), and are well-resolved by our model.

208 The Rossby Number was less than 0.01 in most areas, with values up to 0.1 along the
209 sides of canyons and the coast. This indicates a quasi-geostrophic balance in most areas, strongly
210 influenced by bathymetry.

211 *3.2 Chiniak Trough*

212 Chiniak Trough is a relatively narrow (~10–15 km) and shallow (~110–155 m) regularly
213 shaped trough bounded on each side by shallow (~60 m) banks, and extending ~80 km from
214 Kodiak Island to the continental slope (Fig. 3). In 2001 and 2002, moorings were deployed on
215 either side of the trough. Mean flow at the edges of the trough was largely directed by
216 bathymetry with onshore flow on the northeast and offshore flow on the southwest sides (Fig.
217 3a). The currents were dominated by tides as evidenced from ratios of $KE'/\overline{KE} > 80\%$ (Table 1),
218 and tidal excursions were ~ 10 km.

219 Along the northern bank, during the two summertime deployments bottom flow at CB3
220 had net currents of 10–11 cm s^{-1}, and was directed onshore (Table 1, Fig. 3a). Within the water
221 column, mean flow varied from a minimum of ~9.7 cm s^{-1} at 93 m to a maximum of ~14 cm s^{-1}

222 at ~35 m (Fig. 3b). There was little variability in the vertical profile of currents between the two
223 years (the offset in current direction may have been due to slightly different mooring locations in
224 relation to bathymetry). Along the southern bank, measurements were only made near the
225 bottom, and the mean outflow was weaker (6–8 cm s^{-1}) than the inflow on the northern bank
226 (Fig. 3a). Weaker outflow may have resulted from placement of the moorings just north of the
227 canyon wall (Fig. 3a), or from a portion of the inflow continuing into Chiniak Bay (where CB1 is
228 located) and diverted elsewhere (discussed below).

229 A fortnightly signal was evident in the summer time series, especially in 2002 when daily
230 mean currents beat between 10–20 cm s^{-1} and weak or even reversed flow through the summer
231 (Figs. 3c and 3d). The fortnightly signal was present, but more difficult to identify in 2001 as
232 there were few reversals, and overall net current speeds were lower in summer. Weaker flow in
233 late summer 2001 was not consistent with seasonal variability in the strength of the ACC, which
234 is weakest in June through August (Stabeno et al., 2016a).

235 There were periods when the direction of outflow along the southern bank (i.e. CB2)
236 rotated northward; late July 2001, early June 2002, July 2002 (Figs. 3c, 3d). The cause of these
237 disruptions is not clear, but current rotation was not consistent with the presence of mesoscale
238 eddies. Mesoscale eddies along the slope are common features in this area (Ladd et al., 2007),
239 and satellite SSH measurements revealed a large eddy was present at the mouth of Chiniak
240 Trough in July 2002 (as evident in EKE; Fig. 3d). However, eddies were not present during other
241 periods when outflow currents rotated counter-clockwise (northward) and inflow weakened. It is
242 unlikely that mesoscale eddies were the sole cause of these disruptions.

243 Hydrographic sections in May 2003 (Fig. 4) show the beginning of seasonal warming in
244 surface waters (T > 6°C) with deeper water relatively constant in temperature (~5.8°C). At the

245 bottom of Chiniak Trough, salinity stratifies the water column, especially at the two southern
246 transects. Salinities in the trough decrease from >32.5 near the mouth to <32.3 at the
247 northernmost transect. These sections were completed in ~38 hours on different phases of the
248 tide, and several days prior to the spring tide. At the head of the trough, the water column was
249 well mixed along the northern wall. These results support the idea that mixing occurred primarily
250 at the northern part of the trough, introducing nutrients into the surface layer (Ladd et al., 2005).
251 Salt and nutrients were then injected over shallow banks (Cheng et al., 2012).

252 Chiniak Trough may serve as an important conduit of nutrients and zooplankton into the
253 nursery grounds that are found in Chiniak Bay. A long-term mooring site (1999–present, CB1) is
254 located at the northern extent of Chiniak Trough in Chiniak Bay. Examination of the temperature
255 and salinity near the bottom (~181 m) indicates that it was strongly influence from the surface,
256 and that the water there has undergone mixing (Stabeno et al., 2016a). Bathymetry suggests that
257 the likely source of deep flow into the bay was through Chiniak Trough while flow in Stevenson
258 Trough is the primary source of water into Marmot Bay (Fig. 3a).

259 Daily average currents at CB1 were highly variable with flows exceeding 15 cm s^{-1} for
260 short periods (days) between November and March, with weaker currents occurring in April–
261 August (Fig. 5a). This time series from 2010 was representative of daily velocities from 18 years
262 of data at CB1. Currents in spring and summer were relatively weak, but autumn and winter
263 currents were punctuated with 3–5 day periods of intense flow. Long-term (1999–2014) monthly
264 mean current velocities collected at CB1 show a seasonal signal in bottom currents (Fig. 5b).
265 From September through March currents were westward with a mean velocity of ~4 cm s^{-1}.
266 Velocity decreased in April and the net average velocity was weak in May through June.

267 Near-bottom (~181 m), monthly average velocity and temperature were calculated at

CB1 for 18 years (Fig. 5c). During months with strongest flow (September - March), there was considerable interannual variability in bottom flow. It is unclear if this variability was correlated to inflow at CB3. Although there were marked differences in summertime inflow at CB3 between 2001 and 2002 (Fig. 3c), corresponding flow at CB1 was weak in both years and insufficient to address this question.

Bottom temperatures at CB1 varied seasonally, with maximum temperature occurring in September at the same time that maximum SSTs are observed (discussed below). This in-phase character of bottom temperature and SST is indicative of the strong mixing that occurs in the region bringing surface heat to depth. Interannual variability is evident in temperature with warmer conditions occurring in 1999–2007, and cooler conditions in 2008–2013, with the exception of 2010, when there was a moderate El Niño. Warmest temperatures were observed in 2015 and 2016 during the concurrence of "The Blob" (Bond et al., 2015) and the 2016 El Niño.

3.3 Barnabas Trough

Barnabas Trough and Chiniak Trough are of similar length (~80 km), and the lower portions of the troughs have very similar physical characteristics including orientation to the slope, width (~70 km), and depth (~150 m), although there is a shallow lobe along the eastern bank of Barnabas Trough (Fig. 6). The upper portion of Barnabas Trough is highly irregular with an eastern and central lobe, and a western channel. The western channel is disrupted by several sills and connects to a series of depressions off the southern portion of Kodiak Island (Fig. 1).

In Barnabas Trough, moorings were placed at six locations over a two-year period. Two moorings were deployed on the outer part of the trough, two midway, and two farther up the trough. All moorings were intended to be near the walls of the trough to capture intensified boundary flow; however, three of the moorings (BC2, BC3, and BC4) were, unfortunately,

deployed ~5–10 km away from the wall of the trough and missed the boundary flow. At these mooring sites, net speeds averaged only 2.4 cm s^{-1}. The other three moorings (BC1, BC5, and BC6) captured intensified boundary flow with an average net speed of 9.5 cm s^{-1}, similar to what was measured in Chiniak Trough. The vertical structure of flow at BC1 shows the strong influence of bathymetry (Fig 6b). At this site, net currents increased from 9.5 cm s^{-1} near the bottom (127 m) to 16 cm s^{-1} at 107 m following the bathymetry of the deep trough. Near the surface, the flow weakened (4.7 cm s^{-1} at 11 m) and flowed more eastward along the 100-m isobath, and into a shallow lobe. Current sheer was enhanced at this site relative to BC4 (not shown) and may be an indication of stronger mixing at this site. Farther up the trough (BC5), net current speeds through the water column were less variable, ranging between 6.3 and 10.4 cm s^{-1} (Fig. 6b). It was unclear if differences in flow patterns between BC1 and BC5 were due to spatial or interannual variability. While net bottom flow at BC4 was weak (2.6 cm s^{-1} at 120 m) due to the placement of the mooring (discussed above), the direction of flow was uniform through the water column, and increased in speed to ~8 cm s^{-1} near the surface (Fig. 6b). The almost 10-month records at BC5 and BC6 (Fig. 6c) show a similar spring and summer signal to that at Chiniak Trough; stronger bottom flow from May to August and weaker flow in September. The autumn and early winter data show weaker bottom flow continuing in October and strengthening in November with the breakdown of stratification. Stronger flow persisted at least through January, when the mooring was recovered.

3.4 Mixing in Chiniak and Barnabas Troughs

In Barnabas Trough, $KE'/(\overline{KE} + KE')$ was lower than in Chiniak Trough and other selected mooring sites in the NGOA (Table 1), a result primarily due to weaker tidal energy in Barnabas Trough. These differences in tidal energy were reflected in the response of the vertical

314 temperature structure within Barnabas and Chiniak Troughs (Fig. 7).

315 In Barnabas Trough, while the upper water column (Fig. 7b, red and orange) showed
316 seasonal warming with maximum temperatures in August, waters encompassing the bottom ~60
317 m of the water column (green, blue and purple) showed relatively little summertime (July–
318 September) warming. Bottom temperatures (purple) varied on tidal scales by <1 °C, and there
319 was little warming at depth due to mixing. In August, the ΔT between 17 and 127 m was
320 typically > 5 °C (Fig. 7d, black line).

321 In Chiniak Trough, seasonal warming was evident at all depths with temperatures at 80 m
322 (Fig. 7c, blue) increasing by ~2 °C in July and August, and tidal swings of ~2 °C in bottom
323 temperatures in late summer (purple). Using a small portion of this data, Ladd et al. (2005a)
324 showed that warmer bottom water was associated with ebb tides, presumably due to mixing
325 farther inshore during flood tides that injected warmth and fresher water to depth. As a result, ΔT
326 between 17 and 127 m was generally < 5 °C in August, and occasionally < 2 °C (Fig. 7d).

327 On 21 August 2001, a strong storm (Fig. 7a) mixed the upper ~30 m of the water column,
328 and temperatures at 37 m (orange) increased by ~1.2 °C and 0.8 °C at BC5 and CB3 respectively
329 (Figs. 7b, 7c). Cooler upper waters (17 m) and warmer subsurface waters (~30–40 m) persisted
330 for the remainder of the season. Several days after this mixing event there was a prolonged
331 increase in chlorophyll fluorescence at the mooring site consistent with the injection of nutrients
332 and onset of an autumn bloom (not shown).

333 At BC5, autumn storms and surface cooling weakened stratification, and by early
334 November, the water column temperatures in the upper ~100 m were largely uniform on the ebb
335 tides (~6.7 °C). In mid-November, temperature inversions were commonplace (Fig. 7b).

336 Output from the regional model was used to explore observed differences in mixing

between the two troughs. Modeled temperatures at BC5 (Fig. 8a) and CB3 (Fig 8b) replicate the larger vertical temperature gradient observed at BC5 in summer (Fig. 8e), and the greater extent of deep seasonal warming observed at CB3. The model also replicates enhanced mixing associated with the August 21 storm, with a larger amount of heat mixed to depth at CB3. The smaller temperature gradient at CB3 compared to BC5 (Fig. 8e) is likely due to more intense vertical mixing, driven by the tides. The scalar mixing intensity (Log10 of vertical eddy diffusivity; Figs. 8c, 8d) shows more intense mixing at CB3, especially near the bottom. Note that the quasi-monthly modulation of near-bottom mixing intensity corresponds to the spring-neap cycle of the tides themselves.

3.5 Amatuli Trough

Amatuli Trough lies south of Kenai Peninsula in a region of complex bathymetry and is deeper (>220 m) and wider (30–40 km) than either Barnabas or Chiniak Trough (Figs. 1, 9a). Amatuli Trough extends from the slope toward the Kennedy-Stevenson Entrances, and consists of two basins that are separated by a constriction and sill of ~215 m.

In Amatuli Trough, the net flows from May to September (Fig. 9a) reveal a well-organized bottom flow, with patterns similar to those observed in Chiniak and Barnabas Trough — onshore flow on the north side and offshore flow on the south side. Note that a small-scale bathymetric feature at the location of GB5 directed the inflowing bottom water to the southwest. Higher in the water column the flow at GB5 weakened and turned westward paralleling bathymetry (Fig. 9b). Between GB5 and GB12 the flow in the trough was weaker (GB6 and GB11; Table 1; Fig. 9a). Thus, the stronger flows along the bottom are confined to sides of the trough.

The strongest net flow along the bottom was observed at GB5 (7.6 cm s^{-1}). Weaker

360 bottom flows were observed near the head of the trough (GB13, 4.4 cm s^{-1}) and exiting the
361 trough (GB12, 4.3 cm s^{-1}) (Figs. 9a, 9b). These results suggest that a portion of the bottom inflow
362 circulated and exited the trough while the remainder continued toward the Kennedy-Stevenson
363 Entrances. The flow at these three moorings (GB5, GB12, GB13) were not significantly
364 correlated at the 95% confidence level. Hydrographic sections of salinity across and along the
365 trough show more saline water occurring near the mouth, and fresher water near the head of the
366 trough (Fig. 10). The slope of the halocline in the cross section supports westward flow along the
367 north side of the trough.

368 On the sills north of Amatuli Trough, net bottom flow was weak (GB3, GB4, and GB10).
369 Net bottom flow was greater closer to the Kenai Peninsula (GB1, GB2, GB13, GP34, GP36; Fig.
370 9a), and net flow at GB13 and GP32 increased markedly toward the surface (9 and 24 cm s^{-1},
371 respectively) (Fig. 9b). These results were consistent with observations of the ACC as a surface-
372 intensified flow which extends to the bottom along the Kenai Peninsula at Seward and at Gore
373 Point (see Figures 4 and 5 in Stabeno et al., 2016a).

374 Temporally, the bottom flow at most of the sites was stronger in the autumn and winter
375 than in late spring and summer (Fig. 11), except in the center of the mouth of Amatuli Trough
376 (GB6 and GB11) where currents were relatively weak throughout the year. Seasonal variability
377 in bottom flow was most evident at GB13 and GB36, western moorings that were most likely
378 influenced by the ACC, which has strong seasonality (Stabeno et al., 2016a). All the moorings
379 except GB6 showed freshening beginning in the autumn, though variability at GB6 increased in
380 the fall and winter months. Several different mechanisms are possible causes of this increased
381 variability, including large mesoscale eddies, and seasonal freshening of coastal water upstream
382 of Amatuli Trough followed by mixing of the less saline surface waters downward in autumn.

383 Currents in the trough varied temporally on scales of days to weeks. Multi-year time
384 series at GB5 (Fig. 12) consistently show higher net current speeds in winter as discussed above,
385 but little annual variability in speed and direction. Except for a few short-term reversals each
386 year, net flow along the northern side of Amatuli Trough was directed onshore (westward). In
387 each annual time series, salinity was fresher in winter, likely as a result of vertical mixing by
388 strong winter winds and introduction of fresher surface water deeper in the water column
389 (Stabeno et al., 2004). There is not a clear relationship between current direction and salinity, or
390 between EKE and these parameters.

391 Mesoscale eddies occasionally passed across the mouth of Amatuli Trough, and it has
392 been hypothesized that these eddies influence the salinity of water along the Seward Line
393 (Okkonen et al., 2003) and the transport of plankton into and up the canyon (Coyle and Pinchuk,
394 2005). Satellite images of sea surface height together with time series of near-bottom salinity at
395 GB5, however, illustrate that changes in salinity were not always related to the presence of
396 eddies (Fig. 13; e.g., December 2001, March 2003). In this time series, the source of salinities
397 approaching 34 is likely intrusions of water from the slope (Fig. 10), and seasonal freshening
398 beginning in the late summer and early autumn may be a result of vertical mixing of fresher
399 water upstream of Amatuli Trough.

400 *3.6 Nitrate – Salinity Relationship*

401 To examine the role of submarine canyons in supplying nutrients to the Alaskan Shelf,
402 nitrate+nitrite (hereafter nitrate) analyzers were moored in bottom waters of the NGOA and
403 along the Aleutian Island chain. Moorings were placed near the mouth of Amatuli Trough in
404 2001–2004 (GB5, 188–192 m), near the head of Amatuli Trough in 2002 (GB13, 151 m), in
405 Seguam Pass (far to the west in the Aleutian Islands, 52.134°N, 172.420°W) in 2001 and 2002

406 (151 m), and along the northern bank of Chiniak Trough in 2002 (CB3, 123 m). The nitrate
407 analyzers did not work in all years and all seasons; therefore, a relationship with salinity was
408 developed to estimate seasonal and spatial variability of nitrate. In deeper waters (150-190 m)
409 from Amatuli Trough to Seguam Pass, nitrate and salinity were conserved and linearly related (r^2
410 = 0.82, gray regression line in Fig. 14) according to the function,
411 *Nitrate – 10.66 μM/ppt * Salinity – 325.8 μM* (5)
412 This relationship can be used to assess variability in the cross-shelf flow of nutrients
413 along the path of the Aleutian Stream. In Amatuli Trough, there was relatively little variability in
414 the salinity of inflowing waters (GB5) during summer, ranging from ~33.5 to 33.8 with some
415 fresher events, most notably in July 2001 (Fig. 12). In winter, inflowing water was fresher, but
416 highly variable with salinities occasionally < 32.5. This is equivalent to inflow of 32–35 μM
417 nitrate in summer, and ~20 μM nitrate during freshening events in winter. At the head of Amatuli
418 Trough (GB13, 151 m), nitrate was ~25 μM in summer, decreasing to ~17 μM in winter (based
419 upon measured and derived data using salinities in Fig. 11e and Eq. 5).
420 The data in Fig. 14 largely fall within regression lines from Childers et al. (2005), which
421 were obtained from hydrographic data in 1998 (lower regression line) and 2000 (upper
422 regression line) along the Seward Line at depths of 150–300 m. Nutrient concentrations were
423 lower in 1998 due to warmer El Niño conditions coupled with an anomalously large freshwater
424 discharge in late winter 1998 and early stratification that spring (Childers et al., 2005;
425 Weingartner et al., 2005). While most of the fresher data are coincident with the upper regression
426 line of Childers et al. (2005), in Chiniak Trough the nitrate–salinity relationship was nonlinear
427 due to lower than expected nitrate concentrations associated with fresher water. This non-
428 conservative behavior was the result of deep mixing of fresher, nitrate-depleted surface waters to

429 the bottom of Chiniak Trough, and conversely, injection of deep nutrients into the upper water
430 column to support post-bloom production.

431 **4. Discussion**

432 *4.1 Regional Mixing*

433 Tides play a critical role in structuring the ecosystem, providing energy to mix heat and
434 fresher water downward, and salts and nutrients upward (Ladd et al., 2005a). An impressive
435 feature of the temperature time series were the strong tidal swings in temperatures observed in
436 Chiniak Trough (Figs. 7c, 7d) compared to those in Amatuli Trough (not shown) and Barnabas
437 Trough (Figs. 7b, 7d), especially deeper than 60 m. In Amatuli and Barnabas Troughs,
438 springtime bottom temperatures fluctuated by ~0.6 °C on diurnal tidal scales, but by mid-July,
439 fluctuations of bottom temperatures were <0.1 °C (Fig. 7b). In Chiniak Trough, bottom
440 temperatures often varied several degrees within a diurnal tidal cycle. Due to strong diurnal tidal
441 mixing, ΔT between the shallowest and deepest sensors were occasionally <2 °C (Fig. 7d).
442 Vertical profiles of velocity properties averaged from May to September show that, in summer,
443 current speeds and eddy kinetic energy were especially high in Chiniak Trough relative to
444 Amatuli and Barnabas troughs, and generally increased toward the surface (Supplemental Figure
445 S1).

446 Model output was consistent with these observations (Fig. 8). Because of the greater
447 scalar mixing intensity in Chiniak Trough, modeled temperatures show more heat at depth in
448 Chiniak Trough than in Barnabas Trough. As a consequence, the modeled temperature gradient
449 in the water column ($\Delta T = T_{17} - T_{127}$) was smaller in Chiniak Trough (Fig. 8e), a result
450 consistent with observations (Fig. 7d). While the modeled fortnightly signal in mixing intensity
451 was evident at both sites, there was greater variability in this signal in Chiniak Trough (Fig. 8d).

452 This result is consistent with the large fortnightly swings in bottom temperature observed in
453 Chiniak Trough (Fig. 7c) relative to Barnabas Trough (Fig. 7b). The model also replicates strong
454 mixing observed during the seasonal transition in Barnabas Trough, including temperature
455 inversions in late November.

456 These results build upon results in Ladd et al. (2005a). They examined the tidal pattern in
457 Chiniak Trough for several days in July 2001, and found cooler, more stratified water associated
458 with the flood tide, and warmer, less stratified water during the ebb tide, suggesting more intense
459 mixing toward the head of the canyon. Deviations from the linear nitrate – salinity relationship at
460 CB3 (Fig. 14) provides additional evidence that deep mixing in Chiniak Trough injects nutrients
461 into surface waters in summer thereby sustaining post-bloom production.

462 Compared to the troughs, dissimilar modes of mixing are occurring in the Kennedy-
463 Stevenson Entrances and in Shelikof Strait. Instances of intense shear and mixing have been
464 observed in Kennedy Entrance on fortnightly time scales and were thought to arise from
465 intensified flow of the ACC through this narrow passage (Stabeno et al., 2004). Stevenson
466 Entrance has similar bathymetry and intensified bottom flow (Stabeno et al., 1995), and is likely
467 to be an area with intense vertical mixing, although measurements through the water column
468 (e.g., shear, EKE) were not available.

469 The Shelikof Sea Valley extends from the slope northeastward past Cape Kekurnoi and
470 into Shelikof Strait (Fig. 1). The mouth of the sea valley is deep (>200 m), with a sill (~180 m
471 deep) stretching between Chirikof Island and the Semidii Islands. The width (~40 km) and depth
472 of the sea valley permits a strong onshelf flow along the bottom and southeastern side of the sea
473 valley. In summer, deep inflow extends across the bottom of the sea valley, while in winter it is
474 more episodic and is largely confined to the southern bank (Stabeno et al., 2016a). Inflowing

475 water originates at the slope with little seasonal variability in salinity (~32.9, Stabeno et al.,
476 2004). From Eq. 5, this equates to ~25 μM nitrate in the slope water that fills the bottom of the
477 sea valley in summer.

478 As the northeastward inflow progresses up the sea valley, it is gradually entrained into
479 the southwestward flowing ACC, with mean currents strongest in upper waters along the
480 northern bank, and 6–7 times stronger than the inflow (Reed et al., 1987; Stabeno et al., 2016a).
481 As a result of these patterns, monthly averaged volume transport is always positive (down the sea
482 valley), and varies from 0.2×10^6 m^3 s^{-1} in July to 1.5×10^6 m^3 s^{-1} in January (Stabeno et al.,
483 2016a). The entrainment of cooler, nutrient-rich inflowing deep water into the ACC occurs at
484 mid-depths, and is not necessarily a source to the surface nutrient pool.

485 Satellite imagery of SST revealed relatively cool summertime SSTs over the complex
486 bathymetry surrounding Kodiak Island (Fig. 15a). The coolest temperatures were most often
487 observed in regions of mixing, including Chiniak Trough and the Kennedy-Stevenson Entrances,
488 with warming occurring as these waters flow southwestward down Shelikof Strait. Warmer SSTs
489 were also observed over Middle Albatross Bank where flow is weak. Cooler waters were also
490 observed between Kodiak and the Chirikof Islands, a region that includes shallow banks but
491 were not part of this study. The SST image from August 2003 was representative of summertime
492 SST images, indicating that these are regions of perpetual mixing and nutrient pumping, and
493 sustain high levels of phytoplankton biomass during summer (Fig. 15b; Brickley and Thomas,
494 2004; Hermann et al., 2009; Stabeno et al., 2004).

495 Hydrographic sections taken across Portlock Bank in June 2002 showed increased mixing
496 and nutrients in the vicinity of Portlock Bank (Cheng et al., 2012). They found that by early
497 June, seasonal heating had stratified the upper 50 m in deeper parts of the shelf; however, over

498 Portlock Bank, the water column was well-mixed or only weakly stratified in both temperature
499 and salinity. Drifter tracks (drogued at 40 m) often circulate around Portlock Bank, remaining
500 over the bank for periods of weeks to months (Stabeno et al., 2004, 2016a; Ladd et al., 2005a),
501 and regenerated production may be especially important in regions of closed or semi-closed
502 circulation (Bisagni, 2003). Hence, increased nutrients over the bank may result from sediment
503 re-suspension/remineralization, lateral advection, and from intrusions of nutrient-rich water
504 originating in the troughs.

505 *4.2 Currents*

506 The primary circulation in the coastal GOA is strongly influenced by the local
507 bathymetry, and seasonally-variable winds (Stabeno et al., 2004). The influence of topography in
508 guiding the flow is determined by the ambient stratification and the local current speed
509 (Lagerloef, 1983). For quasi-steady circulation features (those that vary over days to months), the
510 influence of these terms can be gauged using the Rossby Radius length scale and the non-
511 dimensional Rossby Number. The former sets a horizontal length scale for the typical width of
512 features trapped against the coastline or steep bathymetry under stratified conditions, while the
513 latter is a rough measure of how strongly topographic features are expected to steer the low-
514 frequency flow under well-mixed conditions (Gill, 1982).

515 In the coastal GOA, the Rossby Radius varies spatially and seasonally, from larger values
516 in the summer (when stratification is strongest), to smaller values in the winter and over tidally
517 mixed submarine banks (where stratification is weakest) (Fig. 2a). Typical values in the summer
518 range from near zero up to 10 km; the latter value is a typical width of the ACC in Shelikof Strait
519 (Stabeno et al., 2016a). For the canyon flows, the Rossby Number may be used as a measure of
520 the relative influence of the earth's rotation (which tends to make flow follow isobaths through

521 rotational “stiffness”) verses inertia (which tends to keep water parcels on a straight spatial path,
522 ignoring curvature of bathymetry). The small (< 0.1) values exhibited in the canyons indicate
523 substantial topographic steering by those features.

524 Lagerloef (1983) considered topographic steering in Barnabas Trough (at that time called
525 Kiliuda Trough), and through both scaling arguments and quasi-geostrophic modeling concluded
526 that topographic steering by the canyon (which has ~20-km length scale) was significant for low-
527 frequency flows weaker than 10 cm s^{-1}. At higher speeds (i.e. higher Rossby number), inertial
528 forces exceed those due to the earth’s rotation, and the topography of the canyons provides less
529 steering of the flow.

530 In the basin, flow is dominated by the northwestward flowing Alaska Current off
531 southeastern Alaska and by the southwestward flowing Alaska Stream along Kodiak Island and
532 the Aleutian Islands (Stabeno et al., 2004, 2016a, b). This flow provides source waters for inflow
533 in the multiple canyons and troughs that incise the shelf in the NGOA. Within the troughs, near-
534 bottom currents were dominated by tides as evidenced from ratios of $KE'/\left(\overline{KE} + KE'\right) > 80\%$
535 everywhere except in the middle of Barnabas Trough (Table 1). At BC6, net currents were > 12
536 cm s^{-1}, and represented the highest net bottom currents observed at any of the mooring sites
537 during the warm season. Net flow also decreased across Barnabas Trough, but most likely due to
538 mooring placement, as discussed above.

539 Data here and elsewhere (e.g. Ladd et al., 2005a; Stabeno et al., 2004) have been
540 summarized in a schematic showing patterns of bottom flow around Kodiak Island (both
541 observed and implied), and regions of enhanced mixing or entrainment (Fig. 16). These patterns
542 show a well-defined inflow on the right and outflow on the left of the major bathymetric
543 canyons. A portion of flow in Amatuli Trough continues along the Kenai Peninsula and through

544 Kennedy-Stevenson Entrances. This illuminates an important pathway connecting spawning and
545 nursery grounds for some ichthyoplankton.

546 *4.3 Larval Retention and Transport*

547 The physics of this region plays an important role in the distribution of fish eggs and
548 larvae in the pelagic ecosystem subsequent to their release in various spawning locations. A
549 synthesis of four decades of ichthyoplankton data collected 1981–2010 in the GOA includes
550 examination of seasonal progression in distribution and abundance of eggs and larvae of deep
551 water-spawning fish along the continental slope and shelf from Prince William Sound in the
552 north to Unimak Pass in the west (Doyle and Mier, 2016). Emergent patterns indicate the
553 persistence of high concentrations of fish eggs and larvae from deep water spawners along the
554 continental slope region, during winter and spring months, and particularly in association with
555 topographic features such as canyons and troughs that intersect the slope (Doyle et al., 2002;
556 Bailey and Picquelle, 2002; Bailey et al., 2008; Doyle and Mier, 2016). While it is likely that
557 many larvae are "lost" to deep water due to the strong flow associated with the Alaskan Stream,
558 these shelf break locations are characterized by complex bathymetry that can protect planktonic
559 larvae from the strong flow of the Alaskan Stream (Figs. 3, 6, and 9). As larvae develop over a
560 period of weeks to months, ingress of larvae onto the shelf is observed in association with
561 canyons which connect deep water-spawning locations with coastal juvenile nursery grounds.

562 For example, arrowtooth flounder (*Atheresthes stomias*) spawn in winter (peak in
563 January–February) along the slope. By early spring, larvae are still concentrated along the slope
564 with highest concentrations apparent in association with Amatuli Trough, Stevenson Trough, and
565 the mouth of Shelikof Sea Valley (Fig. 17). In half-month intervals from April through May,
566 abundance of larvae is observed to increase in shelf waters, and spatial patterns indicate

567 enhanced onshore transport of larvae through these troughs (Fig. 17; see multiple figures in
568 Doyle and Mier [2016]). Although ichthyoplankton sampling was less intense off the southeast
569 coast of Kodiak Island, relative to the northeast and southwest, ichthyoplankton patterns also
570 indicate enhanced cross-shelf transport of larvae in this region that may be associated with
571 Barnabas and Chiniak Troughs. The influx of early ontogeny stages to shelf and coastal waters is
572 an essential life-cycle feature of many fish species that reside and/or spawn in slope habitats
573 (Doyle et al., 2009; Doyle and Mier, 2012). In addition, certain zooplankton, such as oceanic
574 species of copepods that undergo a diapause stage and then reproduce in deep water (e.g.,
575 *Neocalanus* spp. in the GOA), share this life-cycle feature and their nauplii and early copepodite
576 stages are transported onto the shelf during spring, contributing substantially to the annual spring
577 peak in zooplankton biomass (Coyle et al., 2013).
578 Mechanisms of onshore transport that have been hypothesized previously for various
579 larval fish species in the GOA include eddies along the slope that occasionally mix water onto
580 the shelf, episodic periods of wind-induced downwelling that may transport larvae in surface
581 waters, and bathymetric steering in canyons (Stabeno et al., 2004; Bailey et al., 2008; Atwood et
582 al., 2010). Likely a combination of these different mechanisms contributes to delivery of fish
583 larvae from deep water to coastal regions. Results from the present study, however, illuminate
584 the flow characteristics in the different canyons and troughs that intersect the GOA continental
585 slope and offer clear evidence in support of the importance of these features as conduits for
586 onshore transport of fish larvae and other planktonic organisms. Biological evidence for their
587 importance is provided by the historical ichthyoplankton data, which suggest that deep water-
588 spawning fish with nursery habitat in shelf and nearshore waters (e.g., sablefish (*Anoplopoma*
589 *fimbria*), rockfish species (*Sebastes spp*), and arrowtooth flounder) favor placement of their eggs

590 and larvae in the vicinity of the mouths of these troughs (Doyle and Mier, 2016). As mean flow
591 through the water column in Amatuli Trough is directed toward the Kennedy-Stevenson
592 Entrances (Fig. 9b; Fig 4a in Stabeno et al., 2016a), larvae occurring higher in the water column
593 (upper 30-50 m) are transported across the shelf. Retention of fish larvae from deep water origins
594 on the shelf may be enhanced by conditions such as the eddy-like circulation that is observed
595 over features such as Portlock Bank, where drifters drogued at 40 m have been observed to
596 remain over the bank for weeks to months (Cheng et al., 2012).

597 **5. Summary**

598 The Kodiak Island region is important habitat for many commercially valuable fisheries
599 including walleye pollock (*Gadus chalcogrammus*), Pacific cod (*Gadus microcephalus*), Pacific
600 halibut (*Hippoglossus stenolepis)*, and various species of crab. The region around Kodiak Island
601 exhibits high surface chlorophyll concentrations throughout the summer, while concentrations in
602 surrounding regions show marked reductions after the spring bloom. This high and sustained
603 phytoplankton standing stock could be of importance to zoo- and ichthyoplankton assemblages
604 over the banks themselves, and to living marine resources in the adjacent Kodiak Island region.

605 Patterns of bottom flow were examined in several bathymetric features that incise the
606 shelf around Kodiak Island including Chiniak, Barnabas, and Amatuli Troughs. Introduction of
607 heat, salt, and nutrients into the upper water column is stronger in Chiniak Trough than in
608 Barnabas or Amatuli Trough, but flow in Amatuli is directed toward the strong mixing zones in
609 the Kennedy-Stevenson Entrances. Nutrients advected across the shelf are tidally mixed and
610 injected onto shallow banks, and sustain new production in the region through the summer.
611 Physical and biological data indicate enhanced cross-shelf advection of slope-spawned fish
612 larvae in the canyons and troughs that intersect the slope along the northern to western GOA,

613 delivering them to shelf and nearshore nursery habitats. For instance, hotspots of larval
614 abundance for arrowtooth flounder larvae are consistently associated with Amatuli and
615 Stevenson Trough to the northeast of Kodiak Island as well as outer Shelikof Sea Valley to the
616 southwest. During April and May larval occurrence spreads throughout the shelf, and especially
617 into Shelikof Strait. Historical ichthyoplankton sampling has been less intense in the vicinity of
618 Barnabas and Chiniak Troughs. Nevertheless the seasonal progression in distribution of larval
619 arrowtooth flounder, and larvae of other slope-spawned species, indicates that these troughs also
620 facilitate the cross-shelf transport of early ontogeny stages of fish to the shelf.
621 Results from an individual-based biophysical model in combination with a juvenile
622 habitat suitability model for arrowtooth flounder found that the presence of glacial troughs and
623 valleys were associated with shoreward particle movement and lowered inter-annual variability
624 in settlement success (Goldstein et al., submitted). Furthermore, settlement variability and routes
625 of cross-shelf transport were influenced by the presence and location of retentive eddy features.
626 The implication for fish species that spawn in deep water is that year-to-year variability in
627 delivery of their larvae to shelf and coastal habitats may influence rate of survival to the juvenile
628 stage, and subsequently recruitment to the adult reproducing population.
629

630 **Acknowledgments**

631 We thank the crews and officers of the NOAA ship Miller Freeman and RV Kilo Moana for their
632 assistance and effort. We also thank Bill Floering and Bill Parker for overseeing CTD and
633 mooring operations, Dave Wisegarver for assisting with the nutrient measurements, and Karen
634 Birchfield for assisting with the figures. The “all sat merged” altimeter products were produced
635 by Ssalto/Duacs and distributed by Aviso with support from CNES. This research was

636 generously supported by grants from the NPRB-sponsored GOAIERP (G83), USGLOBEC
637 Program, and NOAA's North Pacific Climate Regimes and Ecosystem Productivity (NPCREP)
638 and Fisheries Oceanography Coordinated Investigations programs. This publication was partially
639 funded by the Joint Institute for the Study of the Atmosphere and Ocean (JISAO) under NOAA
640 Cooperative Agreements NA17RJ1232 and NA10OAR4320148. This research is contribution
641 0842 to NOAA's Ecosystems and Fisheries-Oceanography Coordinated Investigations,
642 contribution 1847 to JISAO, and contribution 4337 to NOAA's Pacific Marine Environmental
643 Laboratory.

644 **References**

645 Aguilar-Islas, A.M., Séguret, M.J., Rember, R., Buck, K.N., Proctor, P., Mordy, C.W., Kachel,
646 N.B., 2016. Temporal variability of reactive iron over the Gulf of Alaska shelf. Deep-Sea
647 Res. II 132, 90–106

648 Atwood, E., Duffy-Anderson, J.T., Horne, J., Ladd, C.A., 2010. Influence of mesoscale eddies
649 on ichthyoplankton assemblages in the Gulf of Alaska. Fish. Oceanogr. 19 (6), 493–507.

650 Bailey, K.M., Picquelle, S.J., 2002. Larval distribution of offshore spawning flatfish in the Gulf
651 of Alaska: Potential transport pathways and enhanced onshore transport during ENSO events.
652 Mar. Ecol. Prog. Ser. 236, 205–217.

653 Bailey, K.M., Abookire, A.A., Duffy-Anderson, J.T., 2008. Ocean transport paths: A comparison
654 of spawning areas, larval distributions and juvenile nurseries of offshore spawning flatfishes
655 in the Gulf of Alaska. Fish and Fisheries 9 (1), 44–66.

656 Bisagni, J.J., 2003. Seasonal variability of nitrate supply and potential new production in the
657 Gulf of Maine and Georges Bank regions. J. Geophys. Res.-Oceans 108 (C11), 8015,
658 doi:10.1029/2001JC001136.

659 Bograd, S.J., Stabeno, P.J., Schumacher, J.D., 1994. A census of mesoscale eddies in Shelikof
660 Strait, Alaska, during 1989. J. Geophys. Res.-Oceans 99 (C9), 18,243–18,254.

661 Bond, N.A., Cronin, M.F., Freeland, H., 2015. The Blob: An extreme warm anomaly in the
662 northeast Pacific. In State of the Climate in 2014, Global Oceans. Bull. Am. Meteorol. Soc.
663 96 (7), S62–S63, doi: 10.1175/2015BAMSStateoftheClimate.1.

664 Boyd, P.W., Law, C.S., Wong, C.S., Nojiri, Y., Tsuda, A., Levasseur, M., Takeda, S., Rivkin, R.,
665 Harrison, P.J., Strzepek, R., et al., 2004. The decline and fate of an iron-induced subarctic
666 phytoplankton bloom. Nature 428, 549–553.

667 Brickley, P.J., Thomas A.C., 2004. Satellite-measured seasonal and inter-annual chlorophyll
668 variability in the Northeast Pacific and Coastal Gulf of Alaska. Deep-Sea Res. II 51 (1–3),
669 229–245.
670 Calkins, D.G., 1986. Marine mammals. In: Hood, D.W., Zimmerman, S.T. (Eds.), The Gulf of
671 Alaska: Physical Environment and Biological Resources. US Department of Commerce,
672 Washington, DC, pp. 527–558.
673 Cheng, W., Hermann, A.J., Coyle, K.O., Dobbins, E.L., Kachel, N.B., Stabeno, P.J., 2012.
674 Macro- and micro-nutrient flux to a highly productive submarine bank in the Gulf of Alaska:
675 A model-based analysis of daily and interannual variability. Prog. Oceanogr. 101 (1), 63–77,
676 doi:10.1016/j.pocean.2012.01.001.
677 Childers, A.R., Whitledge, T.E., Stockwell D.A., 2005. Seasonal and interannual variability in
678 the distribution of nutrients and chlorophyll a across the Gulf of Alaska shelf: 1998–2000.
679 Deep-Sea Res. II 52 (1–2), 193–216.
680 Coyle, K.O., Pinchuk A.I., 2005. Seasonal cross-shelf distribution of major zooplankton taxa on
681 the northern Gulf of Alaska shelf relative to water mass properties, species depth
682 preferences and vertical migration behavior. Deep-Sea Res. II 52 (1–2), 217–245,
683 doi:10.1016/j.dsr2.2004.09.025.
684 Coyle, K.O., Cheng, W., Hinckley, S.L., Lessard, E.J., Whitledge, T., Hermann, A.J., Hedstrom,
685 K., 2012. Model and field observations of effects of circulation on the timing and magnitude
686 of nitrate utilization and production on the northern Gulf of Alaska shelf. Prog. Oceanogr.
687 103, 16–41, doi: 10.1016/j.pocean.2012.03.002.
688 Coyle, K.O., Gibson, G.A., Hedstrom, K., Hermann, A.J., Hopcroft, R.R., 2013. Zooplankton
689 biomass, advection and production on the northern Gulf of Alaska shelf from simulations and

690 field observations. J. Mar. Syst. 128, 185–207.
691 Coyle, K.O., A.J. Hermann, R.R. Hopcroft, in review. Modeled spatial-temporal distribution of
692 production, chlorophyll, iron and nitrate on the northern Gulf of Alaska shelf relative to field
693 observations. Deep-Sea Res. II.
694 Dibarboure, G., Lauret, O., Mertz, F., Rosmorduc, V., Maheu, C., 2010. SSALTO/DUACS User
695 Handbook: (M)SLA and (M)ADT Near-Real Time and Delayed Time Products. AVISO,
696 Ramonville St-Agne, France.
697 Doyle, M.J., Mier, K.L., 2012. A new conceptual framework for evaluating the early ontogeny
698 phase of recruitment processes among marine fish species. Can. J. Fish. Aquat. Sci. 69 (12),
699 2112–2129.
700 Doyle, M.J., Mier, K.L., 2016. Early life history pelagic exposure profiles of selected
701 commercially important fish species in the Gulf of Alaska. Deep-Sea Res. II 132, 162–193,
702 https://doi.org/10.1016/j.dsr2.2015.06.019.
703 Doyle, M.J., Mier, K.L., Brodeur, R.D., Busby, M.S., 2002. Regional variations in springtime
704 ichthyoplankton assemblages in the northeast Pacific Ocean. Prog. Oceanogr. 53 (2-4), 247–
705 282.
706 Doyle, M.J., Picquelle, S.J., Mier, K.L., Spillane, M., Bond, N., 2009. Larval fish abundance and
707 environmental forcing in the Gulf of Alaska, 1981–2003. Prog. Oceanogr. 80 (3–4), 163–
708 187.
709 Ducet, N., Le Traon, P.Y., Reverdin, G., 2000. Global high-resolution mapping of ocean
710 circulation from TOPEX/Poseidon and ERS-1 and -2. J. Geophys. Res.-Oceans 105 (C8),
711 19477–19498.
712 Favorite, F., Ingraham Jr., W.J., 1977. On flow in the northwestern Gulf of Alaska, May 1972. J.

713 Oceanogr. Soc. Jpn. 33, 67–81.
714 Flexas, M.M., Boyer, D.L., Espino, M., Puigdefàbregas, J., Rubio, A., Company, J.B., 2008.
715 Circulation over a submarine canyon in the NW Mediterranean. J. Geophys. Res.-Oceans,
716 113, C12, doi:10.1029/2006JC003998.
717 Gill, A.E., 1982. Atmosphere-Ocean Dynamics (Vol. 30). Academic Press.
718 Goldstein, E.D., Pirtle, J.L., Duffy-Anderson, J.T., Stockhausen, W.T., Zimmermann, M.,
719 Wilson, M.T., Mordy, C.W., Submitted. Eddy retention and seafloor terrain facilitate cross-
720 shelf transport and delivery of fish larvae to suitable nursery habitats.
721 Henson, S.A., 2007. Water column stability and spring bloom dynamics in the Gulf of Alaska. J.
722 Mar. Res. 65 (6), 715–736.
723 Hermann, A.J., Hinckley, S., Dobbins, E.L., Haidvogel, D.B., Bond, N.A., Mordy, C., Kachel,
724 N., Stabeno, P.J., 2009. Quantifying cross-shelf and vertical nutrient flux in the Gulf of
725 Alaska with a spatially nested, coupled biophysical model. Deep-Sea Res. II 56 (24), 2474–
726 2486, doi:10.1016/j.dsr2.2009.02.008.
727 Klinck, J.M., 1996. Circulation near submarine canyons: A modeling study. J. Geophys. Res.-
728 Oceans 101 (C1), 1211–1223.
729 Ladd, C., 2007. Interannual variability of the Gulf of Alaska eddy field, Geophys. Res. Lett. 34
730 (11), L11605, doi:10.1029/2007GL029478.
731 Ladd, C., Stabeno, P.J., Cokelet, E.D., 2005a. A note on cross-shelf exchange in the northern
732 Gulf of Alaska. Deep-Sea Res. II 52 (5–6), 667–679.
733 Ladd, C., Kachel, N.B., Mordy, C.W., 2005b. Observations from a Yakutat eddy in the northern
734 Gulf of Alaska. J. Geophys. Res.-Oceans 110, C03003, doi:10.1029/2004JC002710.

735 Ladd, C., Mordy, C.W., Kachel, N.B., Stabeno, P.J., 2007. Northern Gulf of Alaska eddies and
736 associated anomalies. Deep-Sea Res. 54 (4), 487–509.
737 Lagerloef, G., 1983. Topographically controlled flow around a deep trough transecting the shelf
738 off Kodiak Island, Alaska. J. Phys. Oceanogr. 13 (1), 139–146.
739 Le Traon, P.Y., Dibarboure, G., 2004. An illustration of the contribution of the
740 TOPEX/Poseidon-Jason-1 tandem mission to mesoscale variability studies. Mar. Geod. 27
741 (1–2), 3–13.
742 Le Traon, P.Y., Nadal, F., Ducet, N., 1998. An improved mapping method of multi-satellite
743 altimeter data. J. Atmos. Ocean. Technol. 15, 522–534.
744 Mesinger, F., DiMego, G., Kalnay, E., Mitchell, K., Shafran, P.C., Ebisuzaki, W., Jović, D.,
745 Woollen, J., Rogers, E., Berbery, E.H., et al., 2006. North American regional reanalysis.
746 Bull. Am. Meteorol. Soc. 87 (3), 343–360.
747 Mundy, P.R. (Ed.), 2005. The Gulf of Alaska: Biology and Oceanography. Alaska Sea Grant
748 College Program, University of Alaska Fairbanks, Fairbanks, AK, 220 pp.
749 OCSEAP (Outer Continental Shelf Environmental Assessment Program), 1986. Marine fisheries:
750 Resources and environments. In: Hood, D.W., Zimmerman, S.T. (Eds.), The Gulf of Alaska:
751 Physical Environment and Biological Resources. Ocean Assessments Division, NOAA, U.S.
752 Department of Commerce, Washington, DC, pp. 417–458.
753 Okkonen, S.R., Weingartner, T.J., Danielson, S.L., Musgrave, D.L., Schmidt, G.M., 2003.
754 Satellite and hydrographic observations of eddy-induced shelf-slope exchange in the
755 northwestern Gulf of Alaska. J. Geophys. Res.-Oceans 108 (C2), 3033,
756 doi:10.1029/2002JC001342.
757 Pascual, A., Faugère, Y., Larnicol, G., Le Traon, P.Y., 2006. Improved description of the ocean

758 mesoscale variability by combining four satellite altimeters. Geophys. Res. Lett. 33 (2),
759 L02611, doi:10.1029/2005GL024633.
760 Reed, R.K., 1984. Flow of the Alaskan Stream and its variations. Deep-Sea Res. 31 (4), 369–
761 386.
762 Reed, R.K., Schumacher, J.D., Incze, L.S., 1987. Circulation in Shelikof Strait, Alaska. J. Phys.
763 Oceanogr. 17 (9), 1546–1554.
764 Reed, R.K., Stabeno, P.J., 1989. Recent observations of variability in the path and vertical
765 structure of the Alaskan Stream. J. Phys. Oceanogr. 19 (10), 1634–1642.
766 Royer, T.C., 1982. Coastal fresh water discharge in the northeast Pacific. J. Geophys. Res.-
767 Oceans 87 (C3), 22017–22021, doi:10.1029/JC087iC03p02017.
768 Sambrotto, R.N., Lorenzen, C.J., 1986. Phytoplankton and primary production. In: Hood, D.W.,
769 Zimmerman, S.T. (Eds.), The Gulf of Alaska: Physical Environment and Biological
770 Resources. Ocean Assessments Division, NOAA, U.S. Department of Commerce,
771 Washington, DC, pp. 249–282.
772 Spurgin, J.M., Allen, S.E., 2014. Flow dynamics around downwelling submarine canyons. Ocean
773 Sci. 10, 799–819, doi:10.5194/os-10-799-2014.
774 Stabeno, P.J., Bell, S., Cheng, W., Danielson, S., Kachel, N.B., Mordy, C.W., 2016a. Long-term
775 observations of Alaska Coastal Current in the northern Gulf of Alaska. Deep-Sea Res. II 132,
776 24–40.
777 Stabeno, P.J., Bond, N.A., Kachel, N.B., Ladd, C., Mordy, C.W., Strom, S.L., 2016b. Southeast
778 Alaskan shelf from southern tip of Baranof Island to Kayak Island: Currents, mixing and
779 chlorophyll-a. Deep Sea Res. II 132, 6–23.

780 Stabeno, P.J., Bond, N.A., Hermann, A.J., Kachel, N.B., Mordy, C.W., Overland, J.E., 2004.
781 Meteorology and oceanography of the northern Gulf of Alaska. Cont. Shelf Res. 24 (7–8),
782 859–897.
783 Stabeno, P.J., Reed, R.K., Schumacher, J.D., 1995. The Alaska Coastal Current: Continuity of
784 transport and forcing. J. Geophys. Res.-Oceans, 100 (C2), 2477–2485, doi:
785 10.1029/94JC02842.
786 Strom, S.L., Fredrickson, K.A., Bright, K.J., 2016. Spring phytoplankton in the eastern coastal
787 Gulf of Alaska: Photosynthesis and production during high and low bloom years. Deep Sea
788 Res. II 132, 107–121.
789 Strom, S.L., Olson, M., Macri, E.L., Mordy, C.W., 2006. Cross-shelf gradients in phytoplankton
790 community structure, nutrient utilization, and growth rate in the coastal Gulf of Alaska. Mar.
791 Ecol. Prog. Ser. 328, 75–92.
792 Weingartner, T.J., Danielson, S.L., Royer, T.C., 2005. Freshwater variability and predictability
793 in the Alaska Coastal Current. Deep-Sea Res. II 52 (1–2), 169–191.
794 Zimmermann, M., Benson, J.L., 2013. Smooth sheets: How to work with them in a GIS to derive
795 bathymetry, features and substrates. U.S. Department of Commerce, NOAA Tech. Memo.
796 NMFS-AFSC-249, 52 pp.
797 Zimmermann, M., Prescott, M.M., 2015. Smooth sheet bathymetry of the central Gulf of Alaska.
798 U.S. Department of Commerce, NOAA Tech. Memo. NMFS-AFSC-287, 54 pp.
799

800 Table 1. Near-bottom currents and kinetic energy during May to September for selected
801 moorings in 2001 and 2002 using hourly data. For comparison, data are also shown from
802 Shelikof Strait (February to August). Note that the deepest measurements at SS3 and CB3 were
803 > 40 m off the bottom.

		Mooring	Bottom Depth	Analysis Depth	Net		Maximum Current Speed	Principal Axis		KE'	$\frac{KE'}{(\overline{KE}+KE')}$
					Current Speed	Direction		Mean	Variance		
			(m)	(m)	(cm s^{-1})	(°)	(cm s^{-1})	(°)		(cm^2 s^{-2})	
Chiniak Trough											
2001	NE	CB3	146	97	9.8	306	88	350	80%	293	0.86
	SW	CB2	120	110	5.9	94	68	349	78%	183	0.91
2002	NE	CB3	145	96	10.9	299	67	345	79%	284	0.83
	SW	CB2	112	102	7.7	98	61	348	77%	222	0.88
Barnabas Trough											
Middle - 2001	E	BC5*	142	121	6.3	347	41	4	83%	57	0.74
	W	BC6	128	118	12.3	147	52	4	67%	86	0.53
Lower - 2002	E	BC1	148	127	9.5	25	68	29	97%	186	0.80
Amatuli Trough											
	N	GB5	197	181	7.6	214	70	325	68%	256	0.90
Lower - 2002	Center	GB11	258	222	3.5	270	58	325	68%	341	0.98
	S	GB12	211	181	4.3	134	58	327	77%	191	0.95
Upper - 2002	N	GB13	174	144	4.4	259	70	274	86%	206	0.95
Gore Point											
	N	GP32	157	138	1.9	250	68	279	93%	445	0.996
2002	Center	GP34	145	136	3.3	281	57	281	89%	297	0.98
	S	GP36	187	175	3.7	236	54	298	91%	236	0.97
Shelikof Strait											
	N	SS1	297	270	0.4	55	44	43	88%	42	0.998
Line 8 - 2002	Center	SS2	251	230	2.3	177	80	34	76%	179	0.99
	S	SS3	194	148	4.8	43	73	36	95%	198	0.95

804
805
806 * Originally named BC1, but the placement of BC1 moved in 2002. To avoid confusion, the
807 2001 mooring name has been changed to BC5.

Figures

Figure 1. Bathymetric map of the northern Gulf of Alaska including the location of moorings in Shelikof Strait (SS1, SS2, and SS3), the grid point used for acquisition of modelled wind data (star) from the National Centers for Environmental Prediction (NCEP) North American Regional Reanalysis (NARR), and boxes denoting the region used to determine Eddy Kinetic Energy (EKE).

Figure 2. Bathymetric map of northern Gulf of Alaska showing the first internal Rossby Radius (a) and Rossby Number (b) calculated from model output for mid-July 2010.

Figure 3. Bathymetric map of Chiniak Trough (a) with the location of CTD casts (blue squares), and net bottom currents at CB1 (annual), CB2, and CB3 (May-September). A hodograph (b) indicates net speed and direction of inflow at CB3 at 4 m depth intervals between 16 and 96 m with vectors shown for near-bottom flow. Maximum velocities were at 37 m in 2001 and 32 m in 2002. Time series in 2001 (c) and 2002 (d) of Eddy Kinetic Energy (EKE) determined in a box at the mouth of the trough (see Fig. 1) and daily averaged bottom flow with inflow at CB-3 and outflow at CB-2. The mooring depth and angle of rotation are included with each time series. Gray shading marks the fortnightly tidal frequency.

Figure 4. Four hydrographic sections of salinity (color) and temperature (isotherms) across Chiniak Trough in May 2003. CTD locations are shown in Fig. 2. Irregular ticks along the top of each plot indicate locations of CTD casts.

Figure 5. Time series of bottom flow (181 m) at CB1 (rotated to 270°) of a) daily mean currents in 2010, b) monthly mean currents from 1999-2014, and c) bottom temperature and monthly mean currents from 1999 to 2016.

831 Figure 6. Bathymetric map of Barnabas Trough (a) with net bottom currents for May–September.
832 A hodograph (b) provides net speed and direction of inflow at 4 m depth intervals at BC1
833 (blue, 11–127 m, maximum velocity at 107 m), BC5 (light blue, 12–121 m, maximum
834 velocity at 81 m), and BC4 (red, 12–120 m, maximum velocity at 12 m) with vectors
835 shown for near-bottom flow. Daily averaged bottom flow (c) shows inflow (BC5) and
836 outflow (BC6) in 2001 and early 2002. Currents were not rotated.
837 Figure 7. Time series in 2001: wind stress (a) derived from NARR winds near the mouth of
838 Chiniak Trough (see Fig. 1); temperatures at 10 depths at (b) BC5 in Barnabas Trough
839 and (d) CB3 in Chiniak Trough; temperature difference between 17 m and 127 m at BC5
840 and CB3 (d).
841 Figure 8. Model output from May to November 2001 of temperature profiles at BC5 (a) and CB3
842 (b), profiles of scalar mixing intensity (Log10 of vertical eddy diffusivity) at BC5 (c) and
843 CB3 (d), and the modeled temperature difference between 17 and 100 m at the two
844 mooring sites (e). White indicates values near zero.
845 Figure 9. Bathymetric map of Amatuli Trough (a) with location of CTD casts (blue squares), and
846 mean bottom flow at GB and GP moorings (May to September), a PCP mooring (2012),
847 and the FATE mooring (2004–2005). A hodograph (b) shows the mean flow from May to
848 September 2002 at 4 m depth intervals at GB5 (blue, 33–181 m), GB12 (red, 33–181 m),
849 and GB13 (green, 12–144 m). Vectors are shown for near-bottom flow.
850 Figure 10. Hydrographic sections of salinity oriented across (a, Section ATB) and along (b,
851 Section ATX) Amatuli Trough in May 2001 at CTD locations shown in Fig. 9. Dashed
852 lines indicate the crossing points of those sections.

853 Figure 11. Year-long time series beginning in May 2002 of EKE near the mouth of Amatuli
854 Trough (area shown in Fig. 1) and bottom currents and salinities at six of the mooring
855 sites shown in Fig. 9. Note that the time series for GB6 began in May 2001. The mooring
856 depth and angle of rotation are included with each time series.
857 Figure 12. Time series of EKE near the mouth of Amatuli Trough (area shown in Fig. 1), and
858 daily averaged flow (rotated 230°) and salinity from 2001 to 2004 near the bottom of
859 GB5. The current meter failed during the spring 2003 deployment, and these mooring
860 deployments ceased in October 2004.
861 Figure 13. Images of Sea Surface Height (SSH) on the 15th of each month in the proximity of
862 Amatuli Trough and mooring GB5 (cross). Arrows relate SSH images to time series of
863 bottom salinity at GB5 from May 2001 to April 2003 (2001–2002 top, 2002–2003
864 bottom). The EKE box from Fig. 1 is shown in each image.
865 Figure 14. The relationship between nitrate+nitrite and salinity in Amatuli Trough and Seguam
866 Pass (black symbols and gray regression line), and in Chiniak Trough (red symbols).
867 Dashed blue lines are regressions of hydrographic data from 150 to 300 m along the
868 Seward Line in 1998 (upper line) and 2000 (lower line) taken from Childers et al. (2005).
869 Figure 15. Composite satellite images of (a) Sea Surface Temperature (SST) and (b) Sea Surface
870 Chlorophyll (SS Chlorophyll) in the northern Gulf of Alaska in August 2003.
871 Figure 16. Schematic showing net bottom currents averaged from May to September (observed
872 and implied) in the vicinity of Kodiak Island, and regions of enhanced mixing and
873 entrainment.

874 Figure 17. Spring progression in the distribution of arrowtooth flounder larvae based upon
875 stratified mean abundance of larvae in 20 km^2 grid squares between 1981 and 2010 (from
876 Doyle and Mier, 2016).

877
878

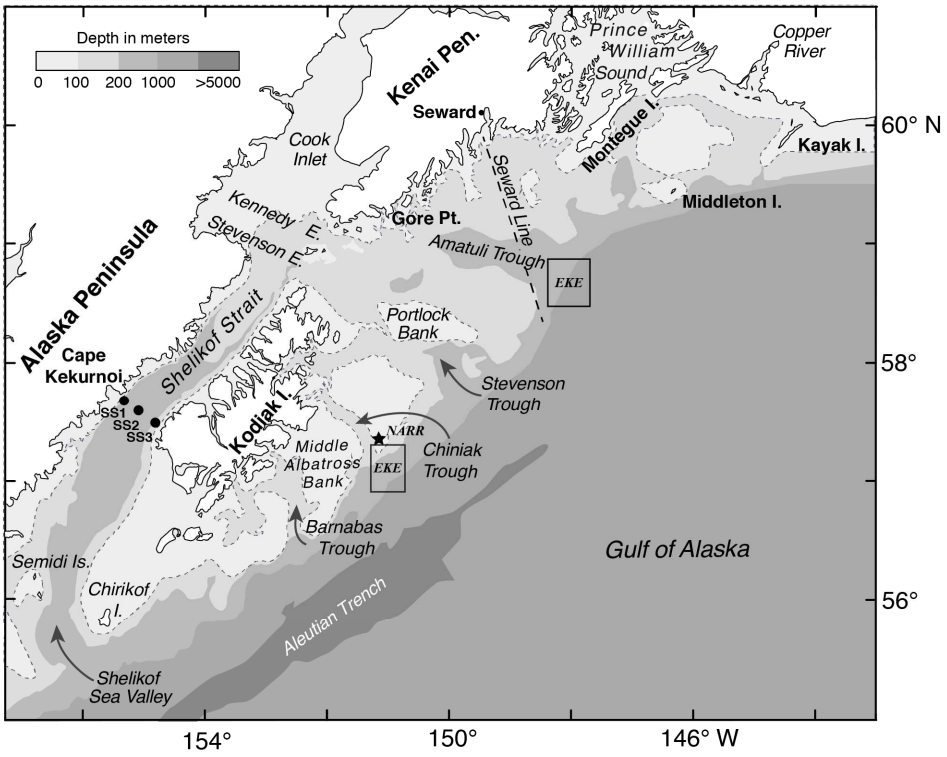

879
880
881
882 Figure 1

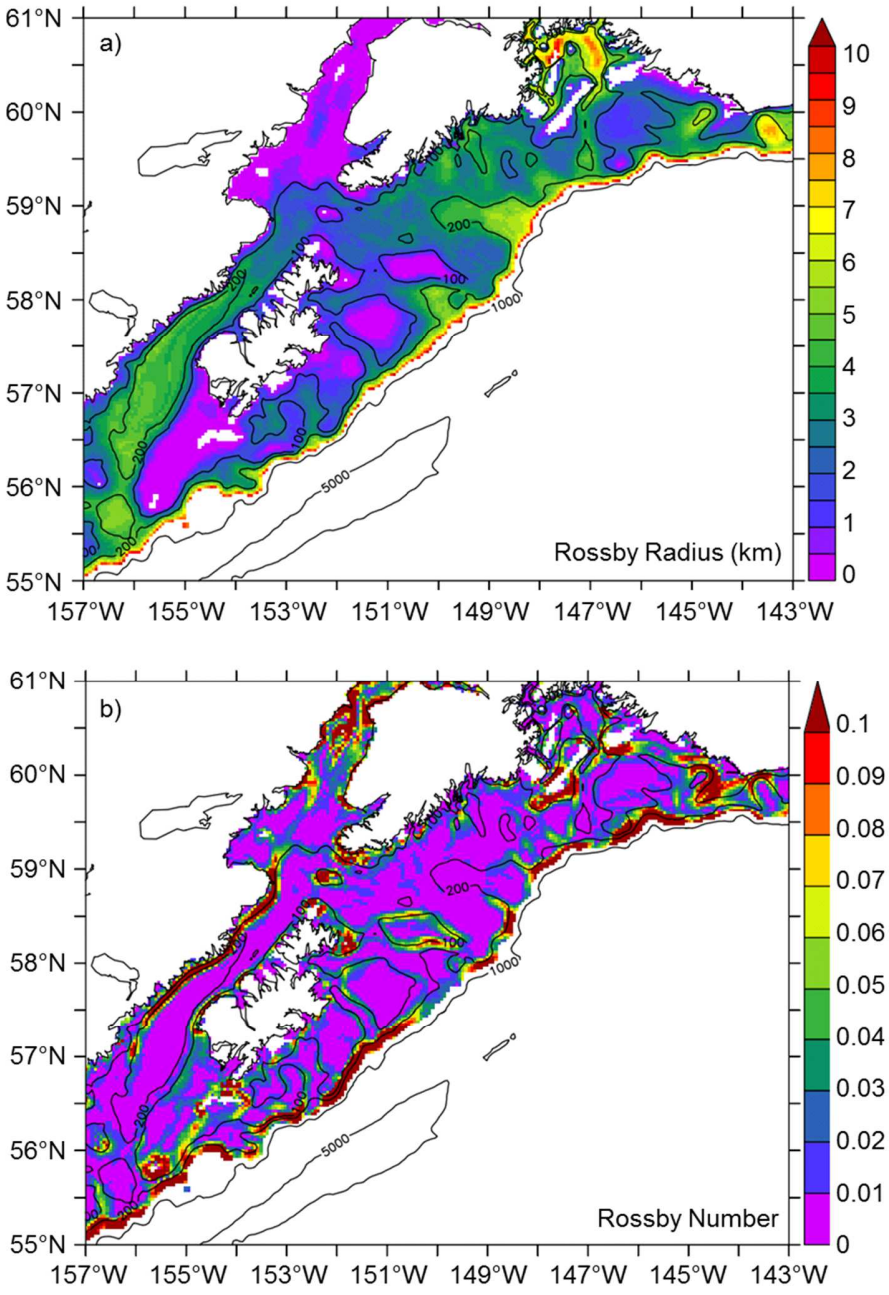

883
884
885 Figure 2

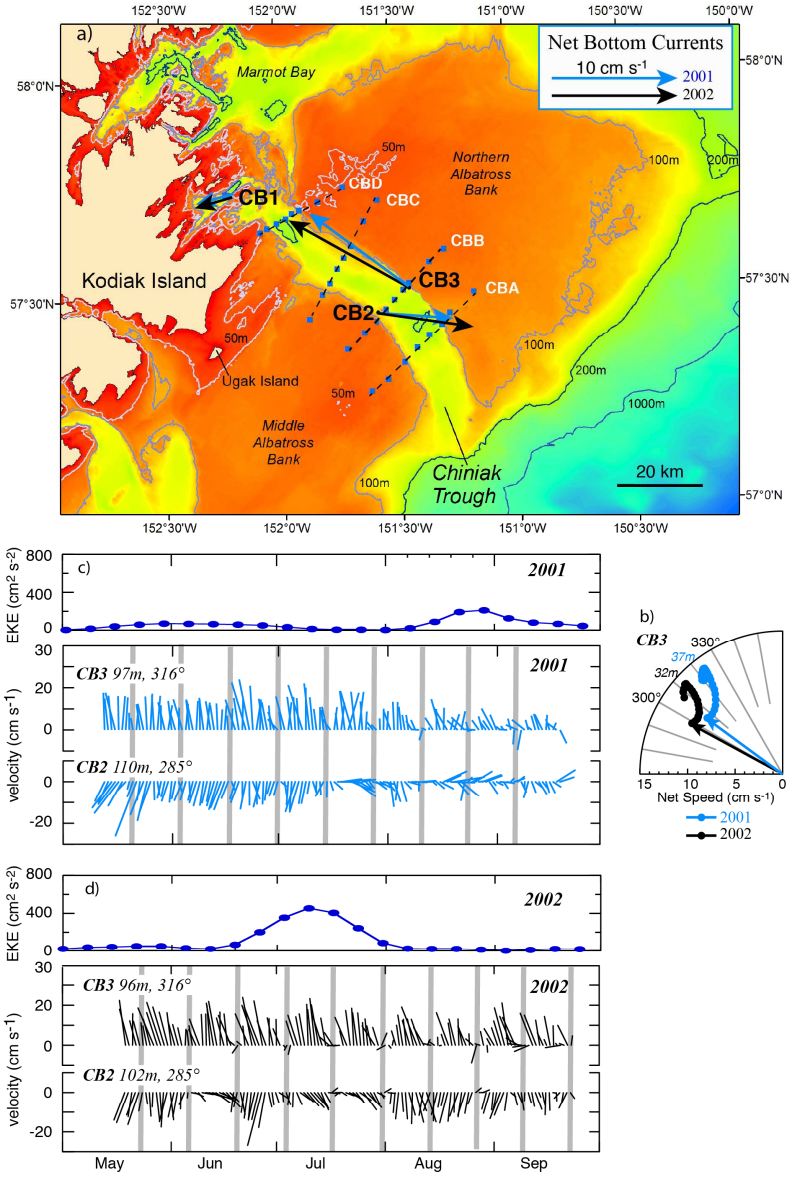
a)
Net Bottom Currents
10 cm s-1
2001
2002
Marmot Bay
Northern Albatross Bank
CB1
CBD
CBC
CBB
CB3
CBA
CB2
Kodiak Island
Ugak Island
Middle Albatross Bank
Chiniak Trough
20 km
152°30'W
152°0'W
151°30'W
151°0'W
150°30'W
150°0'W
58°0'N
57°30'N
57°0'N
50m
100m
200m
1000m
c)
2001
EKE (cm2 s-2)
CB3 97m, 316°
CB2 110m, 285°
velocity (cm s-1)
b)
CB3
330°
37m
32m
300°
15
10
5
0
Net Speed (cm s-1)
2001
2002
d)
2002
CB3 96m, 316°
CB2 102m, 285°
May
Jun
Jul
Aug
Sep

Figure 3

890

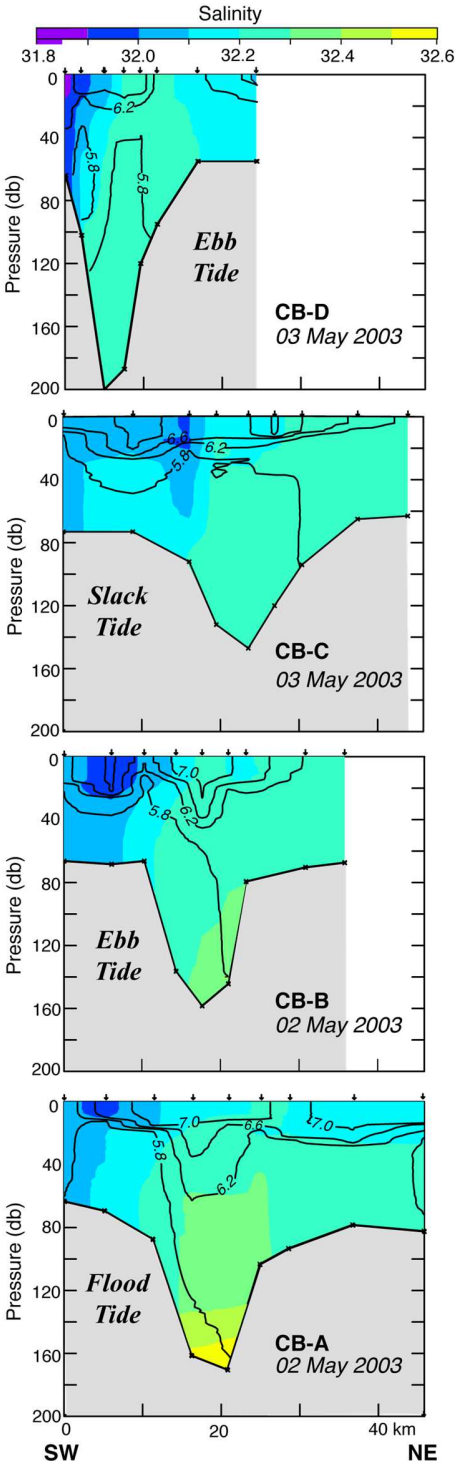

891
892

893 Figure 4

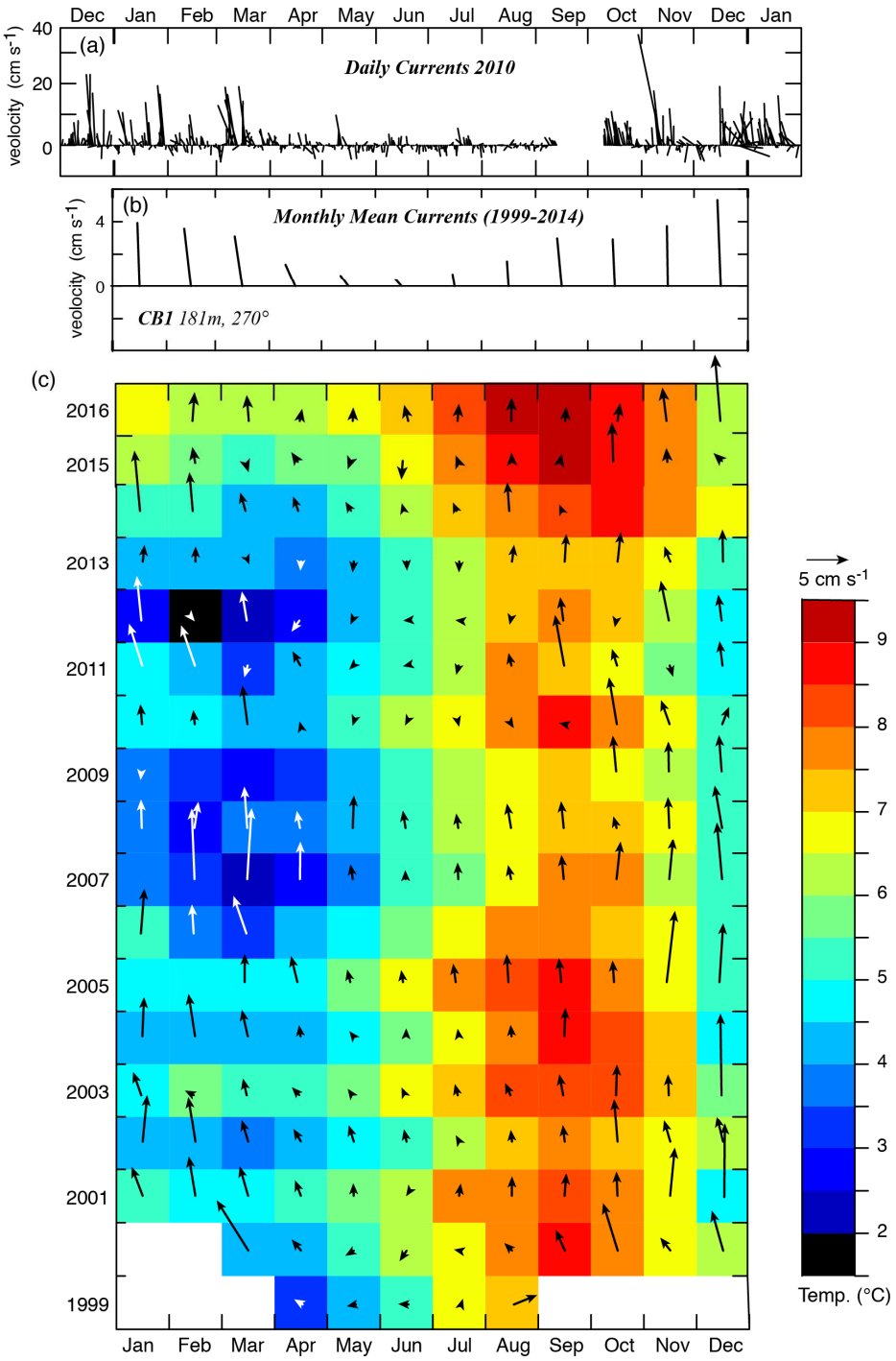

894
895
896
897 Figure 5
898

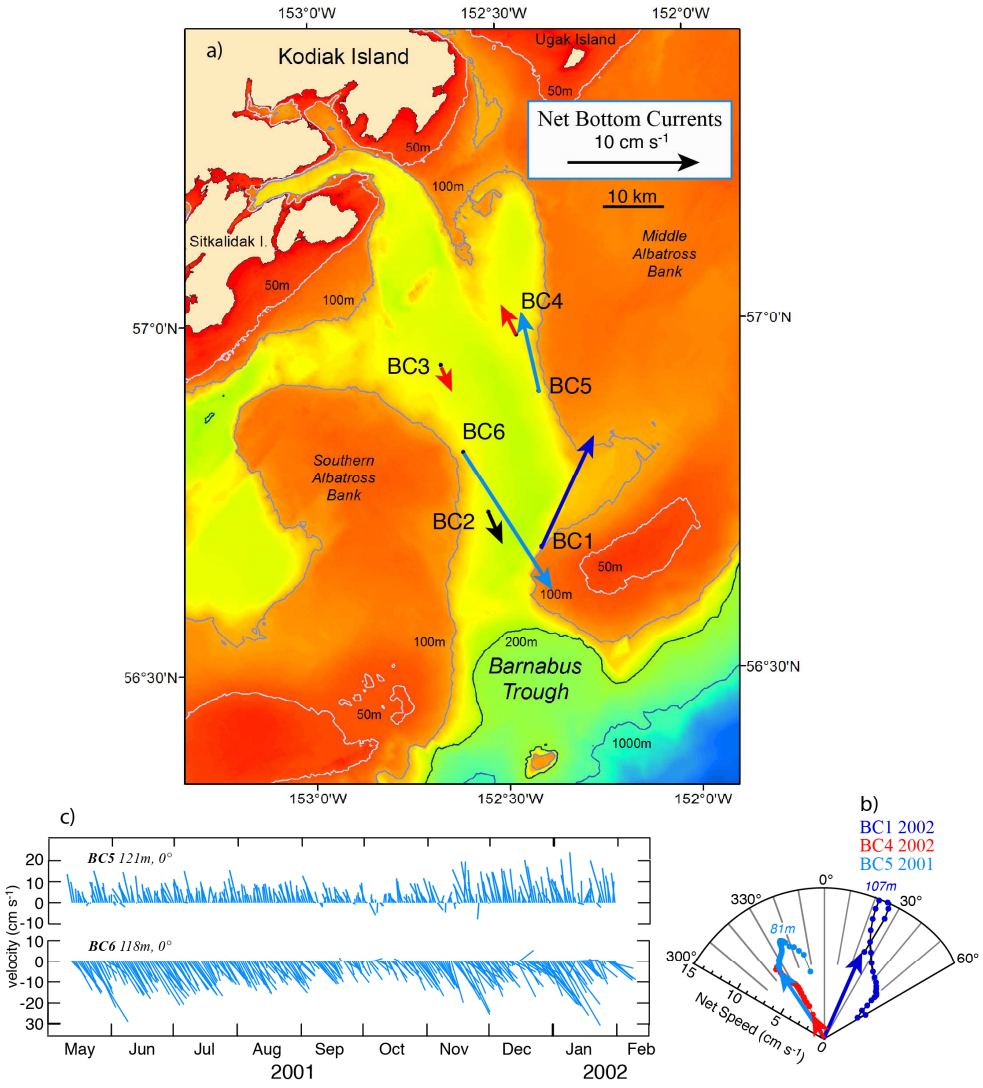

899
900
901 Figure 6
902
903

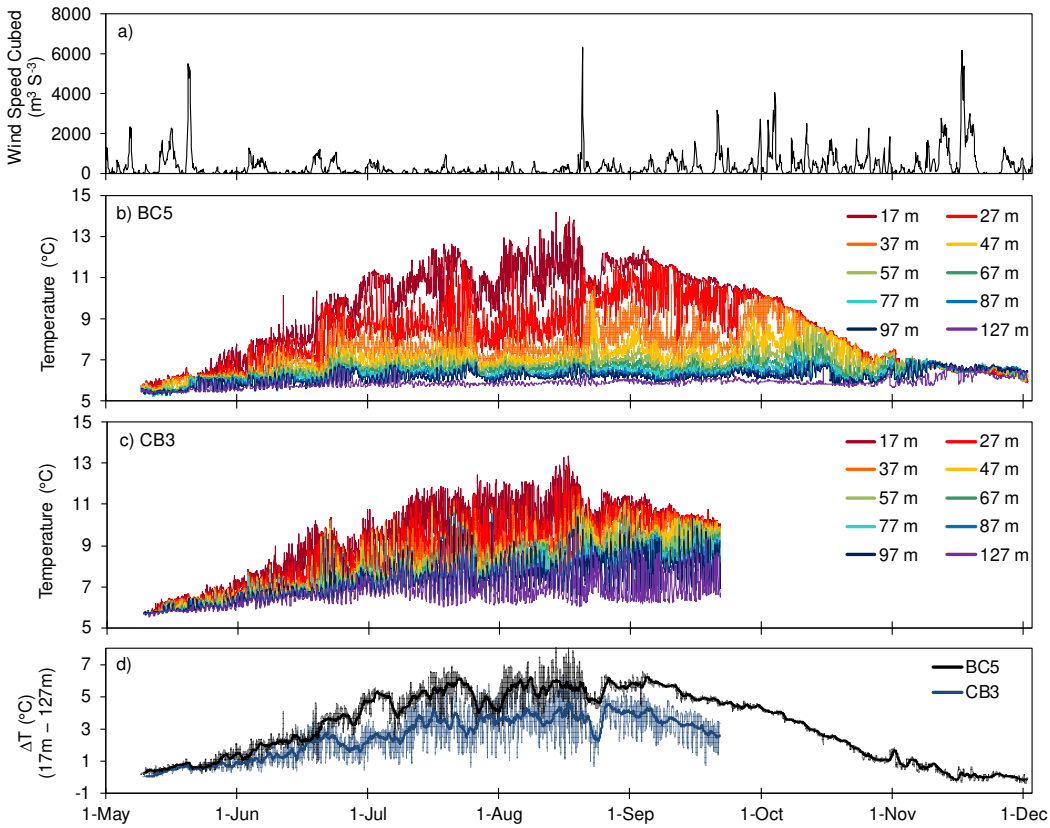
a)
Wind Speed Cubed (m3 S-3)
8000
6000
4000
2000
0
b) BC5
Temperature (°C)
15
13
11
9
7
5
17 m
27 m
37 m
47 m
57 m
67 m
77 m
87 m
97 m
127 m
c) CB3
Temperature (°C)
d)
ΔT (°C) (17m – 127m)
7
5
3
1
-1
BC5
CB3
1-May
1-Jun
1-Jul
1-Aug
1-Sep
1-Oct
1-Nov
1-Dec

Figure 7

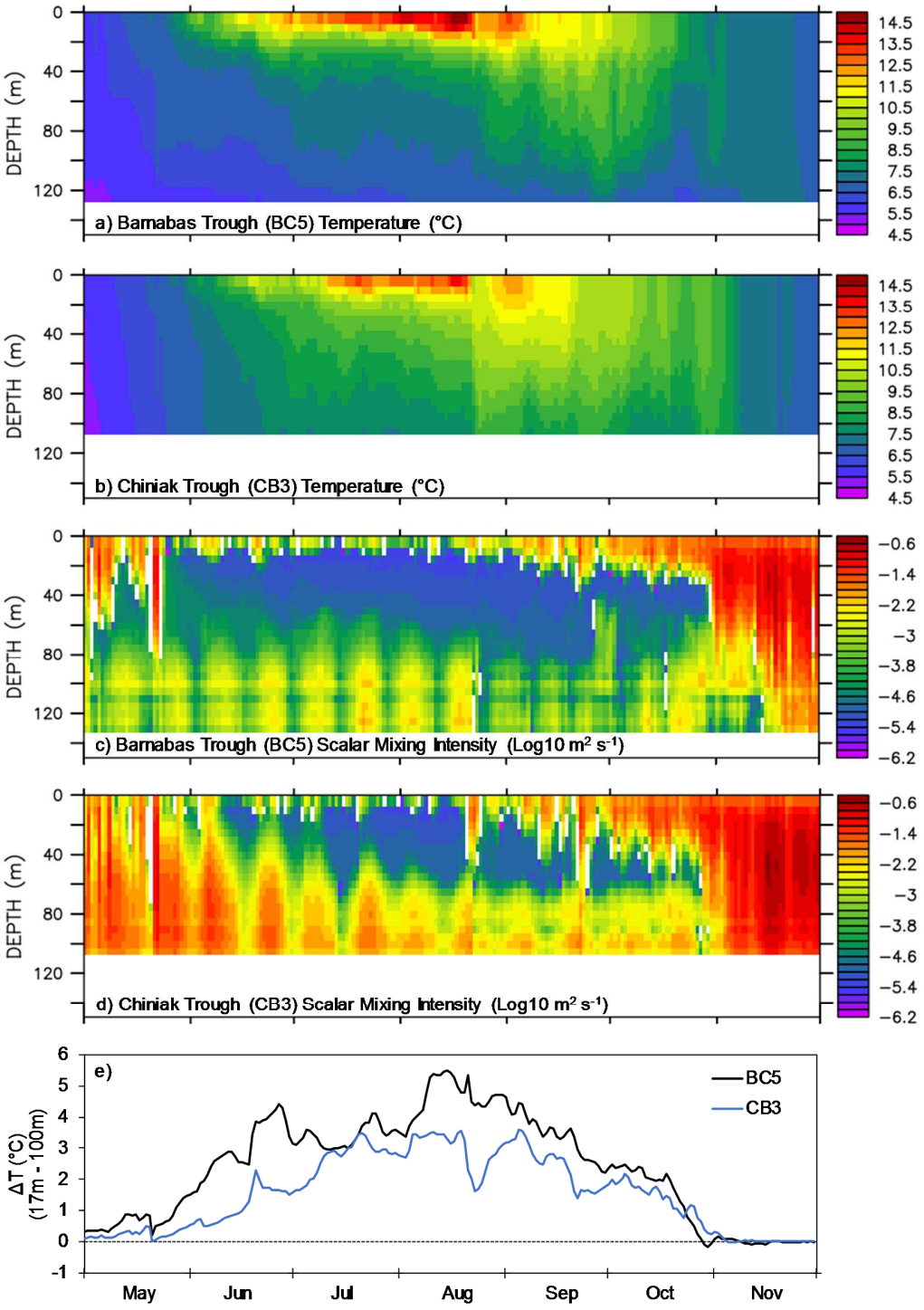
DEPTH (m)
0
40
80
120
a) Barnabas Trough (BC5) Temperature (°C)
14.5
13.5
12.5
11.5
10.5
9.5
8.5
7.5
6.5
5.5
4.5
b) Chiniak Trough (CB3) Temperature (°C)
c) Barnabas Trough (BC5) Scalar Mixing Intensity (Log10 m² s⁻¹)
−0.6
−1.4
−2.2
−3
−3.8
−4.6
−5.4
−6.2
d) Chiniak Trough (CB3) Scalar Mixing Intensity (Log10 m² s⁻¹)
e)
BC5
CB3
ΔT (°C)
(17m - 100m)
6
5
4
3
2
1
0
-1
May
Jun
Jul
Aug
Sep
Oct
Nov

Figure 8

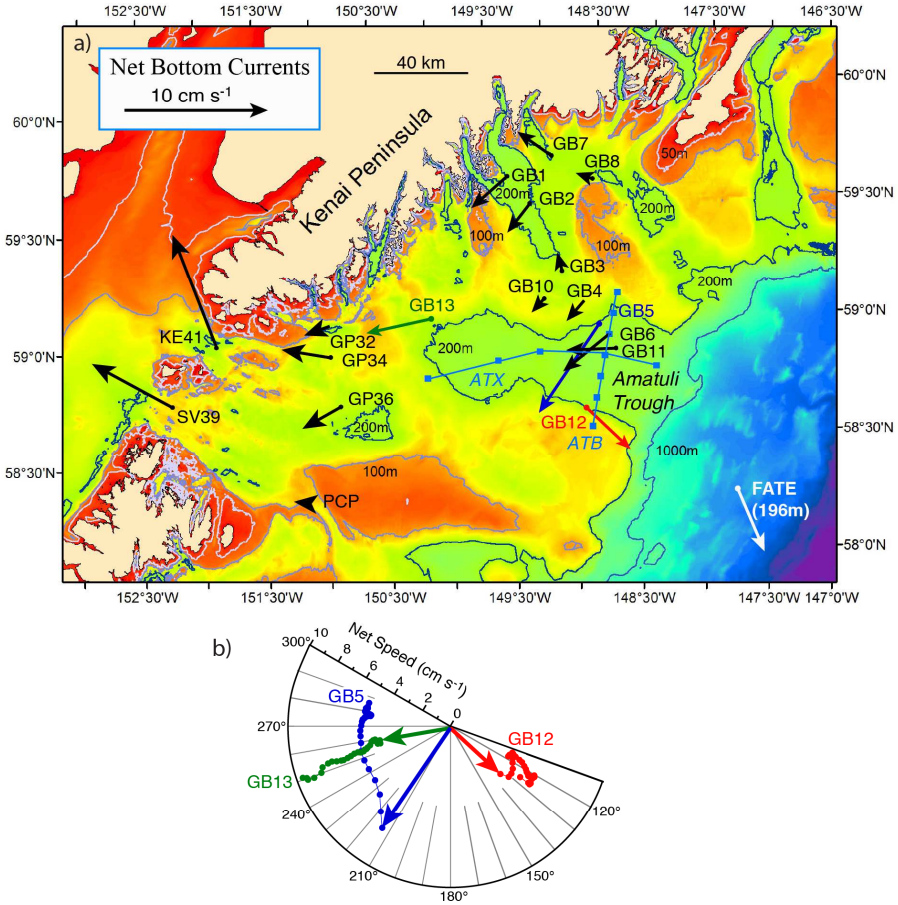

912
913
914 Figure 9

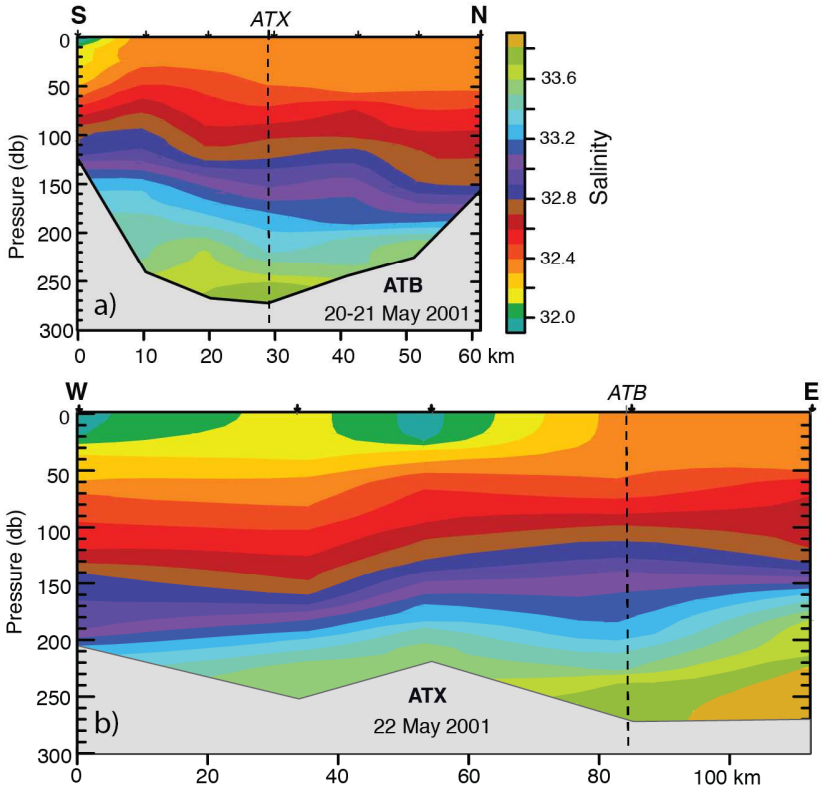
S
ATX
N
Pressure (db)
0
50
100
150
200
250
300
a)
ATB
20-21 May 2001
0
10
20
30
40
50
60 km
33.6
33.2
32.8
32.4
32.0
Salinity
W
ATB
E
Pressure (db)
b)
ATX
22 May 2001
0
20
40
60
80
100 km

Figure 10

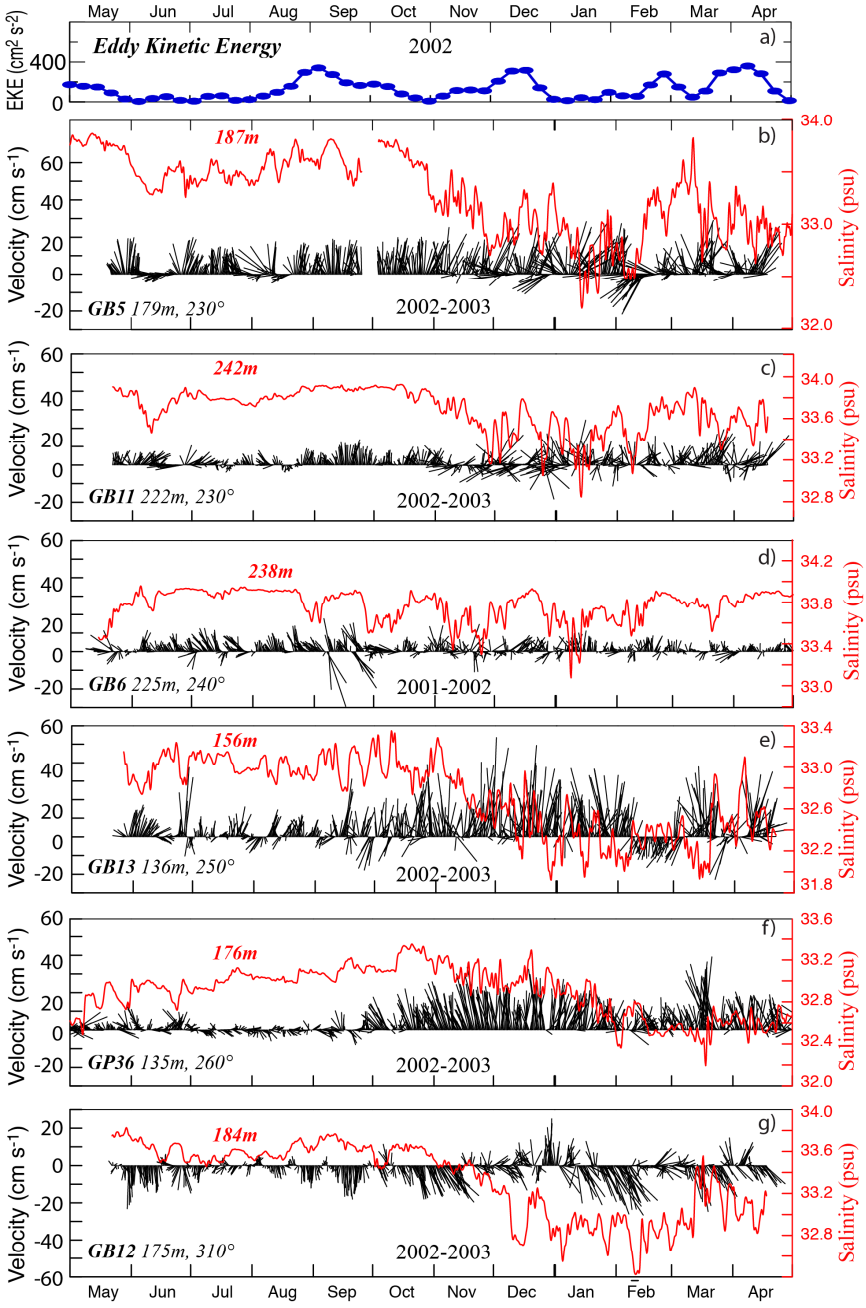
May Jun Jul Aug Sep Oct Nov Dec Jan Feb Mar Apr
Eddy Kinetic Energy
2002
a)
EKE (cm² s⁻²)
400
0
187m
b)
Velocity (cm s⁻¹)
Salinity (psu)
GB5 179m, 230°
2002-2003
242m
c)
GB11 222m, 230°
2002-2003
238m
d)
GB6 225m, 240°
2001-2002
156m
e)
GB13 136m, 250°
2002-2003
176m
f)
GP36 135m, 260°
2002-2003
184m
g)
GB12 175m, 310°
2002-2003

Figure 11

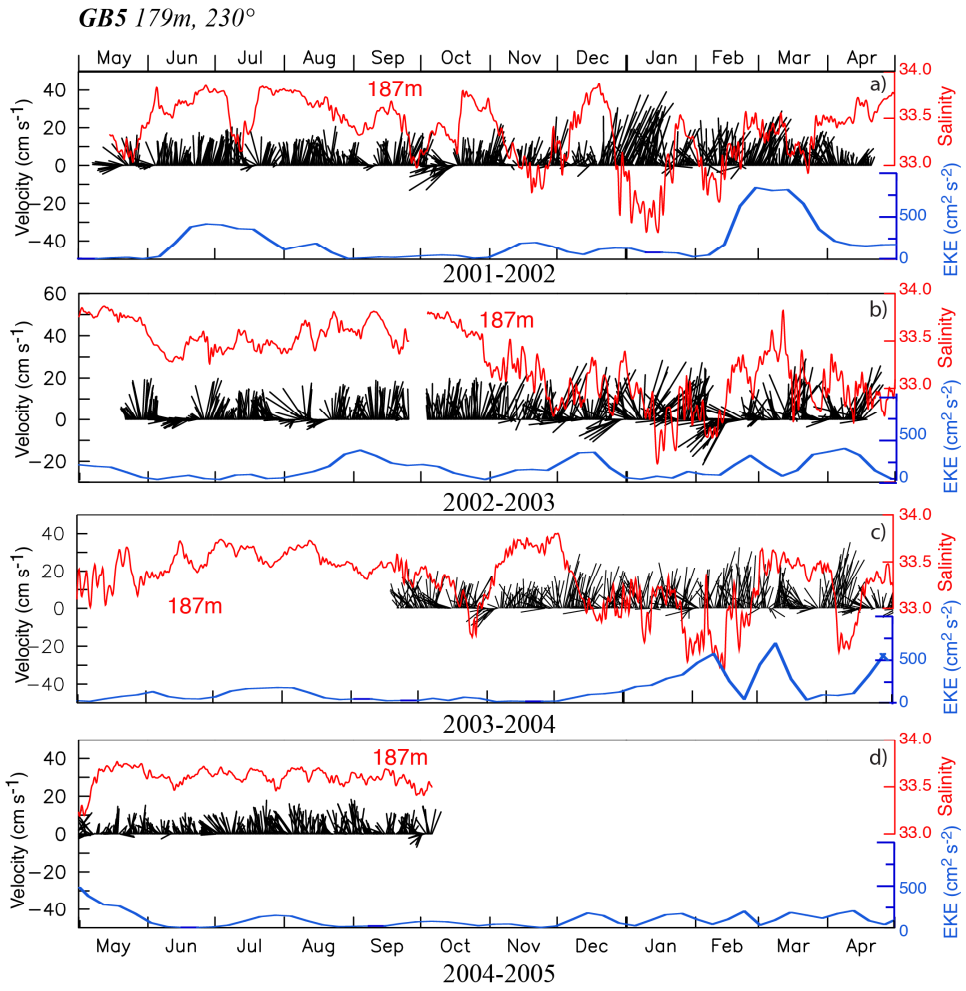

927
928
929
930 Figure 12

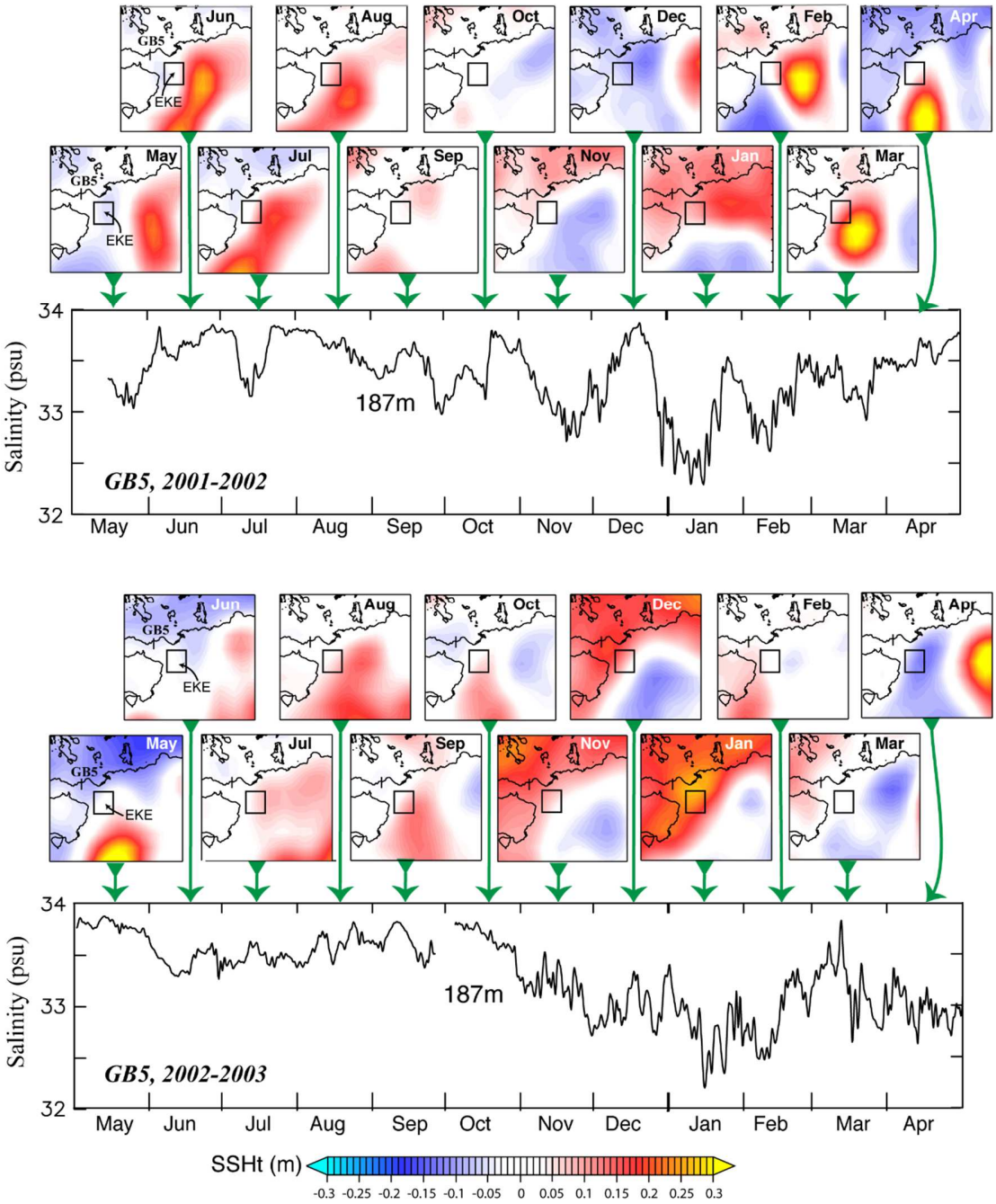

931
932
933 Figure 13

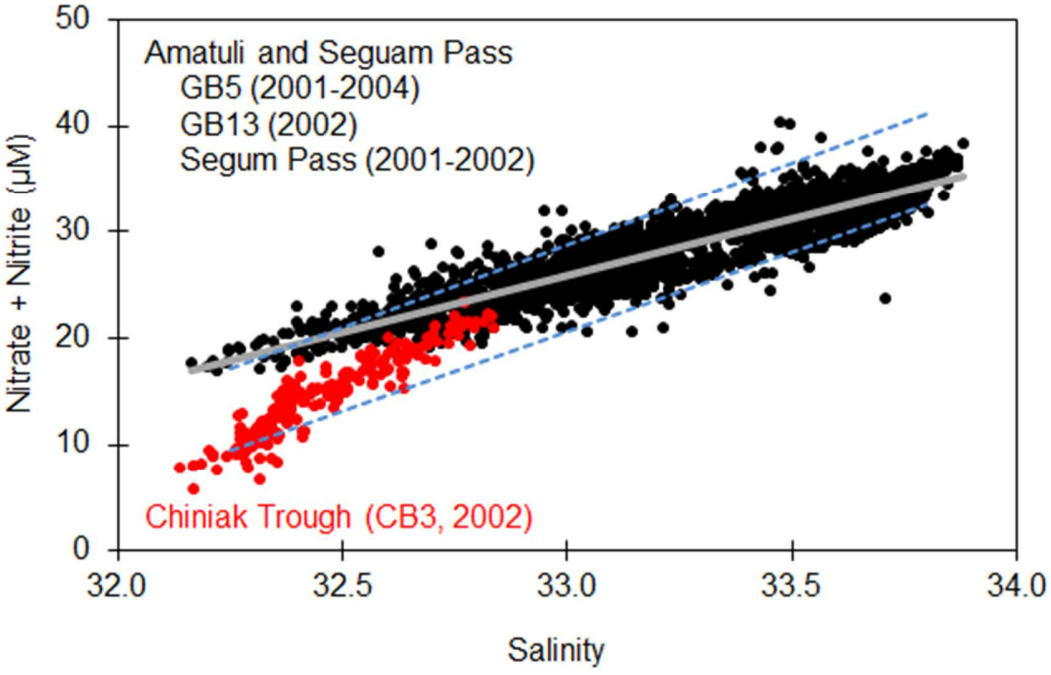

934
935
936 Figure 14

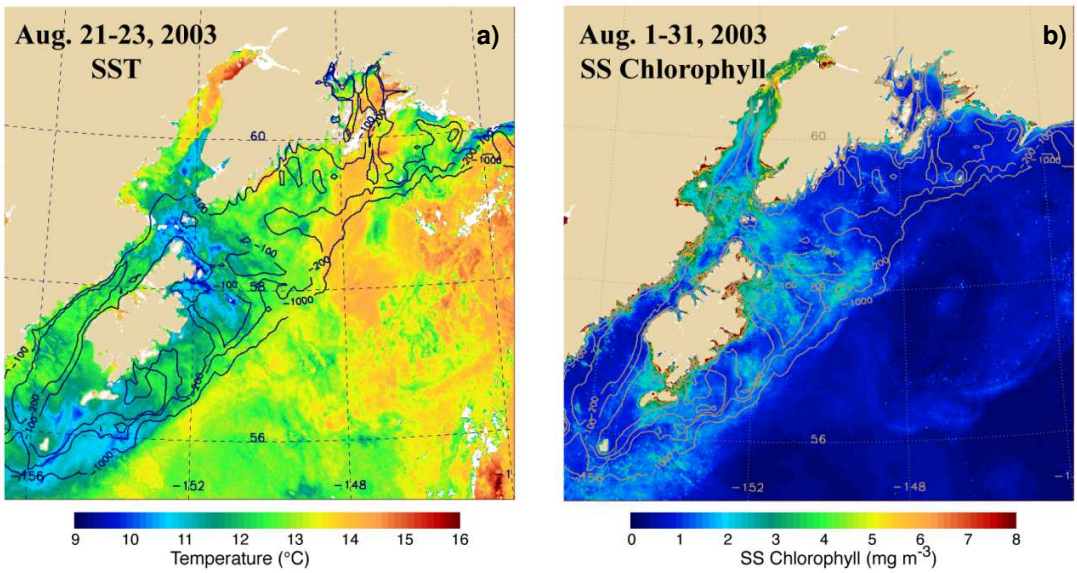
Aug. 21-23, 2003
SST
a)
9 10 11 12 13 14 15 16
Temperature (°C)
Aug. 1-31, 2003
SS Chlorophyll
b)
0 1 2 3 4 5 6 7 8
SS Chlorophyll (mg m-3)

Figure 15

960

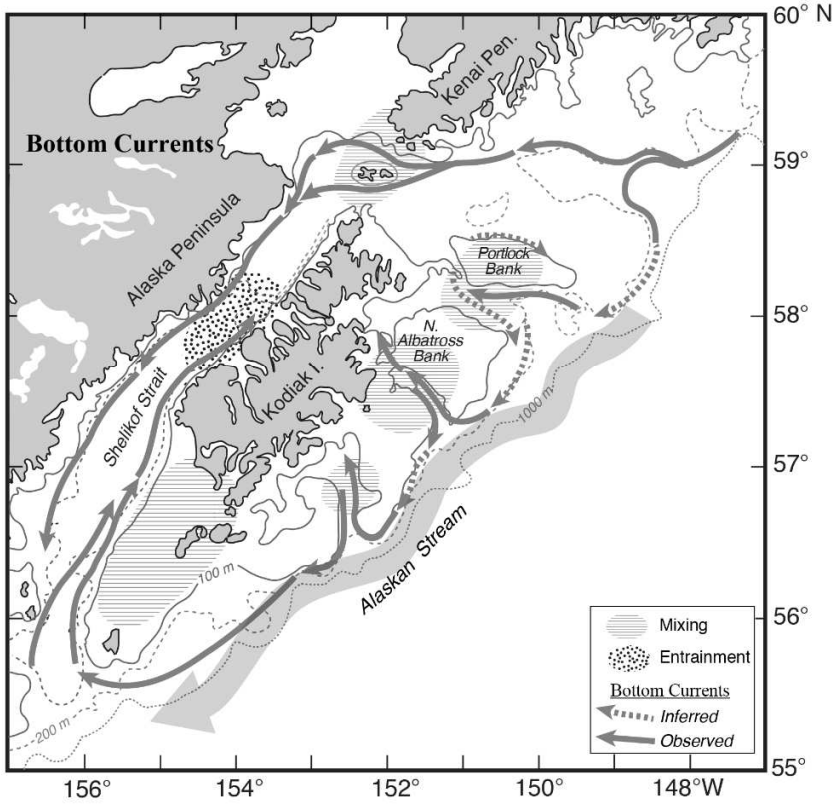

961
962
963
964 Figure 16
965
966

967

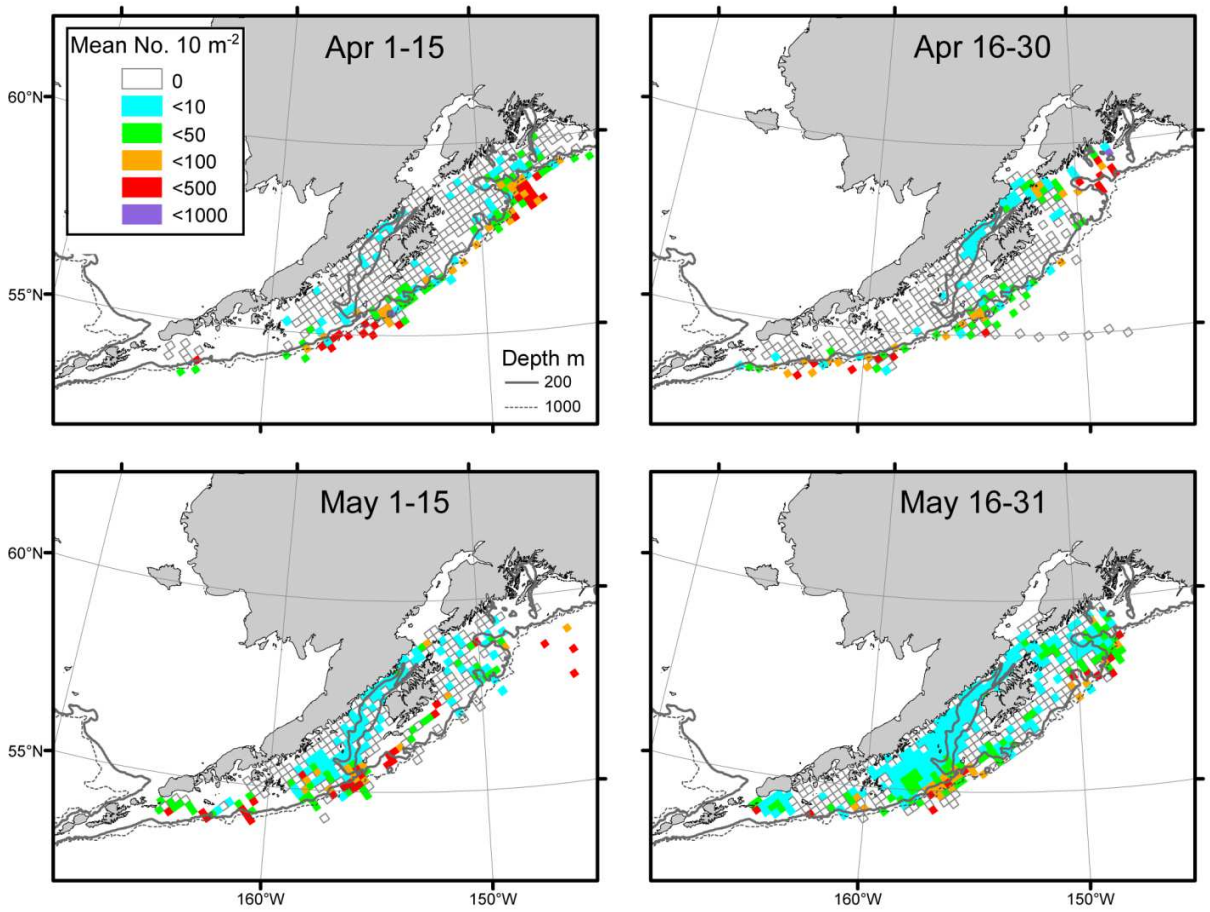

968
969
970
971 Figure 17
972
973
974

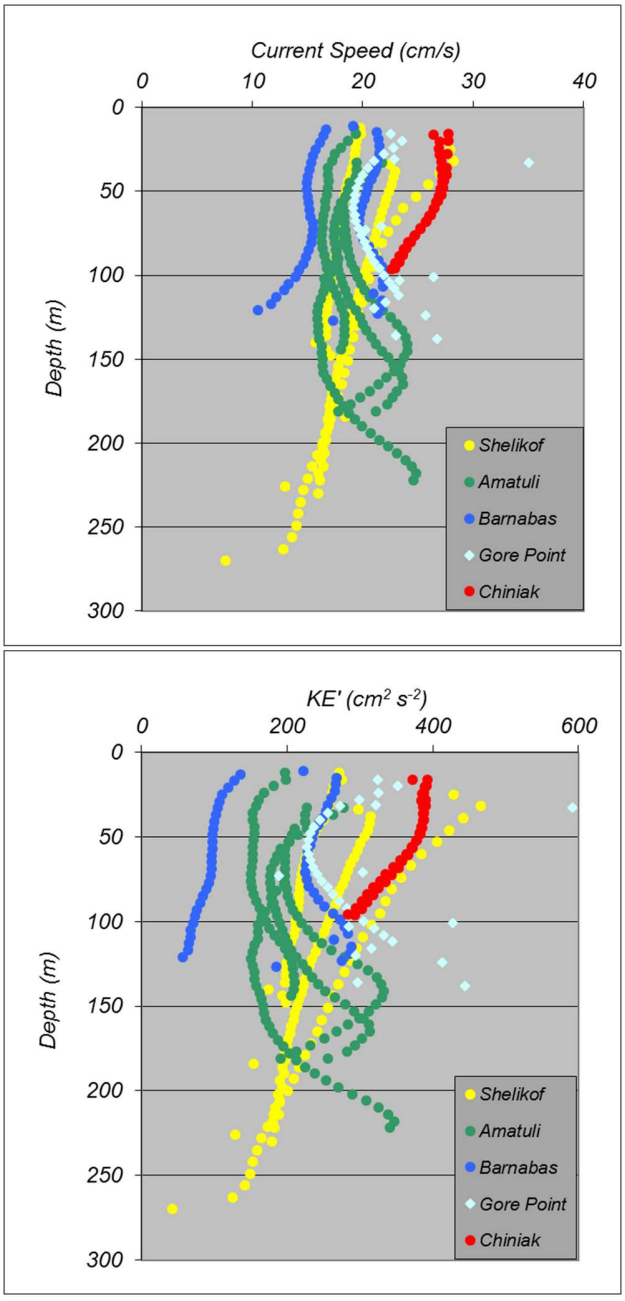

975
976
977 Figure S1. Vertical profiles of mean current speed (top) and KE´ (bottom) for all moorings listed
978 in Table 1 except CB2, BC1 and BC5 as these sites only had measurements at the bottom.